

The Intercomparison of Radiation Codes Used in Climate Models: Long Wave Results

ROBERT G. ELLINGSON

Department of Meteorology, University of Maryland, College Park

JAMES ELLIS

Lawrence Livermore National Laboratory, University of California, Livermore

STEPHEN FELS¹

Geophysical Fluid Dynamics Laboratory, Princeton, New Jersey

An international program of intercomparison of radiation codes used in climate models has been initiated because of the central role of radiative processes in many proposed climate change mechanisms. During the past 6 years, results of calculations from such radiation codes have been compared with each other, with results from the most detailed radiation models (line-by-line models) and with observations from within the atmosphere. Line-by-line model results tend to agree with each other to within 1%; however, the intercomparison shows a spread of 10–20% in the calculations of radiation budget components by the less detailed climate model codes. The spread among the results is even larger (30–40%) for the sensitivities of the codes to changes in radiatively important variables, such as carbon dioxide and water vapor. The analysis of the model calculations shows that the outliers to many of the clear-sky calculations appear to be related to those models that have not tested the techniques used to perform the integration over altitude. When those outliers are removed, the agreement between narrow band models and the line-by-line models is about $\pm 2\%$ for fluxes at the atmospheric boundaries, about $\pm 5\%$ for the flux divergence for the troposphere, and to about $\pm 5\%$ for the change of the net flux at the tropopause as CO₂ doubles. However, this good agreement does not extend to the majority of the models currently used in climate models. The lack of highly accurate flux observations from within the atmosphere has made it necessary to rely on line-by-line model results for evaluating model accuracy. As the intercomparison project has proceeded, the number of models agreeing more closely with the line-by-line results has increased as the understanding of the various parameterizations has improved and as coding errors have been discovered. The most recent results indicate that several climate model techniques are in the marginal range of (relative) accuracy for longwave flux calculations for many climate programs. However, not all such models will give such accuracy. It is recommended that a code not be accepted to provide such accuracy until it has made comparisons to the line-by-line results of this study. The data necessary to make such comparisons are included herein. However, uncertainties in the physics of line wings and in the proper treatment of the water vapor continuum make it impossible for the line-by-line models to provide an absolute reference for evaluating less-detailed model calculations. A dedicated field measurement program is recommended for the purpose of obtaining accurate spectral radiance rather than integrated fluxes as a basis for evaluating model performance.

1. INTRODUCTION

The initial focus of the Intercomparison of Radiation Codes Used in Climate Models (ICRCCM) was on comparisons of clear-sky longwave radiation calculations, and a workshop to discuss preliminary results of the clear-sky longwave study was held in Frascati, Italy (August 1984) [see *World Meteorological Organization* (WMO), 1984; Luther *et al.*, 1988]. At the time of the Frascati Workshop, 39 separate sets of results had been received from 28 research groups, but few modelers completed all of the then 37 test cases. The results of those calculations are summarized by WMO [1984] and Luther *et al.* [1988]. The major findings of the

workshop were the large spread of results for the same input data and the scarcity of accurate observations of known quality with which to evaluate models. Thereafter, the study followed the course of testing models with techniques that employ the most fundamental physics and evaluate the necessary equations with high numerical accuracy (i.e., line-by-line models).

The Frascati workshop identified some problem areas requiring new calculations, and it specified a set of calculations for the cloudy-sky study. Some of the new results were discussed at a second workshop at the University of Maryland in March 1986. The discussions at the workshops identified problems in some codes, such as outmoded spectral data or coding errors, and it was decided to allow the participants approximately 1 year to modify their results if they thought necessary. Furthermore, as the results of the Frascati workshop became known, other scientists became interested in participating in the model intercomparison. Therefore a call for additional participants was made in order to have more results for the cloudy-sky study and to include more groups making calculations with climate applications (i.e., surface and top of the atmosphere radiation budgets).

¹Deceased, October 22, 1989.

The ICRCM leadership was reorganized after Dr. Luther's death, and the window for participation in the comparison was held open until April 1, 1988. Several of the Frascati participants modified their results, a few were withdrawn, and 10 new groups submitted results. In total, 38 research groups contributed 41 sets of results for the now 55 clear-sky cases, although few completed all of the test cases. The participants and their affiliations are listed in Table 1.

In general, the spread of the new ensemble set of calculations is very close to that seen at the Frascati workshop and discussed by *Luther et al.* [1988]. However, the distributions have changed in a direction that more models now agree better with the line-by-line results. This paper is directed at summarizing those re-

sults and offering explanations for the differences between model calculations.

Because the purely calculational phase of ICRCM is drawing to a close, it is important to document many of its important details so that others might participate in the future and advance the current state-of-the-art of modeling longwave radiative transfer. However, in order to appreciate many of the results, it is necessary for the reader to understand the differences in the general approaches to modeling. Section 2 describes the various approaches. Section 3 summarizes the various test cases. Section 4 presents the results of our analysis of many of the clear and cloudy test cases. Conclusions and future plans for ICRCM are summarized in section 5.

2. APPROACHES TO MODELING

2.1. Assumptions and Basic Equations

The principal frequency integrated quantities being compared include the upward flux component, the downward flux component, and the net (upward minus downward) flux at the surface, tropopause, and top of the atmosphere. For this study the atmosphere is assumed to be a plane parallel, horizontally homogeneous medium in local thermodynamic equilibrium. The integral equations that describe the flux components for such an atmosphere are well known [e.g., *Rogers and Walshaw*, 1966], and many different numerical techniques have been used by the ICRCM participants to evaluate the various flux components.

The types of integrals that must be evaluated are illustrated by the equation for the clear-sky (no scattering) downward flux at altitude z , written as

$$F \downarrow(z) = - \int_0^{\infty} d\nu \int_z^{z_t} \pi B_\nu(z') \frac{\partial T_{F\nu}(z, z')}{\partial z'} dz' \quad (1)$$

where ν is frequency or wave number (the reciprocal of wavelength), B_ν is the Planck function for the temperature at altitude z' , z_t is the effective top of the atmosphere, and $T_{F\nu}$ is the flux transmissivity defined as

$$T_{F\nu}(z, z') = 2 \int_0^1 T_\nu(z, z'; -\mu) \mu d\mu \quad (2)$$

where μ is the cosine of zenith angle. For one absorbing gas of density ϱ_a , the monochromatic transmissivity T_ν , for the slant path from z' to z along μ , is related to the monochromatic absorption coefficient k_ν as

$$T_\nu(z, z'; -\mu) = \exp \left(- \int_z^{z'} k_\nu \varrho_a \frac{dz''}{\mu} \right) \quad (3)$$

Physically, equation (1) states that the downward flux at z is due to the sum of the contributions of each emitting element between z and the top of the atmosphere, each attenuated by the appropriate optical path. The equation for the upward flux component has similar terms.

Because of the nearly discontinuous variation of the absorption coefficient with ν , the integration over ν poses significant practical problems for the computation of clear-sky radiation

TABLE 1. Participants Who Contributed Model Calculations to the Clear and/or Cloudy Sky Studies

Participant	Affiliation
A. Arking	NASA Goddard Space Flight Center, USA
J.-P. Blanchet	Canadian Climate Center, Canada
B. Briegleb	National Center for Atmospheric Research, USA
R. D. Cess	State University of New York at Stony Brook, USA
A. Chedin	Laboratoire de Meteorologie Dynamique, France
M.-D. Chou	NASA Goddard Space Flight Center, USA
P. Downey	National Center for Atmospheric Research, USA
R. G. Ellingson	University of Maryland, USA
J. S. Ellis	Lawrence Livermore National Laboratory, USA
E. M. Feigelson	USSR Academy of Sciences, Moscow, USSR
S. Fels	Geophysical Fluid Dynamics Laboratory (GFDL), Princeton University, USA
J.-F. Geleyn	Direction Meteorologie Paris, France
S. Goldenberg	Atmospheric and Environmental Research, Inc., USA
S. Ghan	Lawrence Livermore National Laboratory, USA
H. Grassl	Universitat Kiel, FRG
S. Gupta	NASA Langley Research Center, USA
Harshvardhan	Purdue University, USA
I. Karol	Main Geophysical Observatory, USSR
J. Kiehl	National Center for Atmospheric Research, USA
D. Kratz	NASA Goddard Space Flight Center, USA
W. Kuhn	University of Michigan, USA
I. Laszlo	University of Maryland, USA
A. Lacis	NASA Goddard Institute for Space Studies, USA
K.-N. Liou	University of Utah, USA
J.-J. Morcrette	European Center for Medium Range Weather Forecasts (ECMWF), United Kingdom
R. E. Newell	Massachusetts Institute of Technology, USA
F. Nieuwstadt	Royal Netherlands Meteorological Institute., The Netherlands
S. Ou	University of Utah, USA
V. Ramanathan	University of Chicago, USA
E. Raschke	Institute fur Geophysik und Meteorologie, Koln, FRG
B. Ritter	ECMWF, United Kingdom
B. Rockel	Institut fur Geophysik und Meteorologie, Koln, FRG
M. E. Schlesinger	Oregon State University, USA
P. Schlussel	Universitat Kiel, FRG
J. Schmetz	European Space Operations Center, FRG
M. D. Schwarzkopf	GFDL, Princeton University, USA
N. Scott	Laboratoire de Meteorologie Dynamique, France
K. Schine	University of Oxford, United Kingdom
A. Slingo	U. K. Meteorological Office, United Kingdom
J. Slingo	ECMWF, United Kingdom
E. Smith	Florida State University, USA
T. Suttles	NASA Langley Research Center, USA
S. Tjemkes	Royal Netherlands Meteorological Institute, The Netherlands
K. R. Vupputuri	Canadian Climate Center, AES, Canada
W.-C. Wang	Atmospheric and Environmental Research, Inc., USA
R. Wetherald	GFDL, Princeton University, USA
W. Wiscombe	NASA Goddard Space Flight Center, USA

quantities. The next two sections summarize the types of techniques commonly used to perform this integration. This is followed by a discussion of problems associated with the other integrals.

2.2. Line-by-Line Technique

The most straightforward, but most computer time consuming, technique is to specify k_v at sufficiently small intervals (10^{-4} to 10^{-2} cm^{-1}). This is no small task because k_v depends on the locations, strengths, and shapes of the spectral lines throughout the spectrum. Specifically, k_v may be written as

$$k_v(T, p) = \sum_J S_J(T) f_J(T, p, \nu_{\alpha J}, \nu) \quad (4)$$

where S_J is the integrated line intensity for the J th line, f_J is the line shape factor for the line centered at $\nu_{\alpha J}$ for temperature T and pressure p . Because this technique involves summing the contributions of each spectral line, it is usually called the line-by-line technique (LBL). Details concerning variations of this technique may be found in the works by Drayson [1967], Fels and Schwarzkopf [1981] and Scott and Chedin [1981].

Use of the LBL technique has become more widespread with the availability of documented spectral line data [e.g., McClatchey et al., 1973] and high speed computers. However, because of the large number of lines in the spectrum (order of 10^5), the LBL technique consumes copious amounts of computer time on the fastest computers when applied to flux and heating rate calculations. As a result, it is not a technique useful for routine calculations in climate models.

In the absence of appropriate field measurements, line-by-line model results represent the best available benchmarks, but their use as calibration standards raises several questions. First, one may ask how well the basic spectroscopic properties are known. The line intensities are linked to laboratory measurements of total band and line absorption and to theoretical models of the strengths of molecular transitions. The line compilations change from time to time as better data arise. Generally, however, the line intensities for the atmospheric gases H_2O , CO_2 , and O_3 are believed to be known to within 5 to 10% for the strongest lines in the most recent compilation by the Air Force Geophysical Laboratories (AFGL) [Rothman et al., 1987].

The line shape factor determines how the line absorption is spread over frequency, and its functional form depends upon assumptions concerning relative roles of Doppler and pressure broadening. The ICRCCM LBL models generally used the mixed Lorentz-Doppler (Voigt) profile, although different line shape assumptions were made by each investigator. For example, for CO_2 the line wings are sometimes parameterized to decay more rapidly than the Lorentz formula to take into account observed variations of the line profile.

In practice, LBL models usually do not include the effects of lines beyond a given distance from the line centers because of the uncertainties in line shapes. This usually is adequate to account for the effects of local lines, but this neglects the cumulative effects of strong distant lines. For gases like CO_2 , this is not a major problem. However, for water vapor, the effects of the distant lines may dominate the effects of the local lines in regions of weak absorption. This effect forces modelers to add an additional absorption coefficient to equation (4), which is generally referred to as "continuum absorption."

One may ask how well the various ICRCCM LBL calculations agree with each other. As we shall discuss next, intercode agree-

ment is generally quite good, and often excellent. There is always the possibility, however, that this is simply a reflection of elimination of important code errors (a nontrivial task), and mutual use of a common set of unverified assumptions. In fact, this may well be a serious problem, as we shall see.

Figure 1 displays the cooling rates calculated for the ICRCCM mid-latitude summer (MLS) atmosphere (discussed below) by two of the principle LBL groups: the NASA Goddard Laboratory for Atmospheres (GLA) and the Geophysical Fluid Dynamics Laboratory (GFDL). These two codes are not identical; among other things, they differ in the manner in which the frequency integration is done, the vertical quadrature scheme employed, and in the precise assumptions made about the far-wing shape of Lorentzian lines. Nevertheless, it will be seen immediately that the results generally agree very well, to within 0.1 K/d in most regions. This is characteristic of these two codes, and gives us considerable confidence that given the "canonical" common assumptions about gross line shapes and intensities, we can calculate cooling rates with considerable accuracy.

While the agreement is heartening, it must be observed that there are several important assumptions made in common by

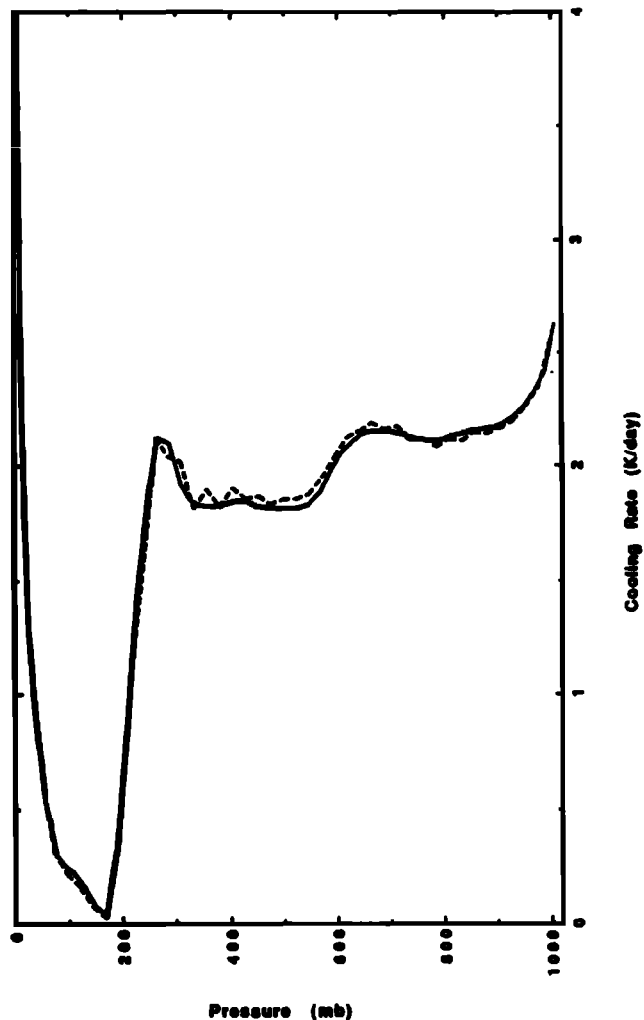


Fig. 1. A comparison of cooling rates calculated with line-by-line models developed at the Geophysical Fluid Dynamics Laboratory (solid) and the NASA Goddard Laboratory for Atmospheres (dashed). The calculations use 300 ppmv CO_2 , and the H_2O , O_3 , and temperature distributions of the mid-latitude summer atmosphere.

both models which require careful investigation. In particular, both use intensities and widths taken from various versions of the AFGL compilation. More important, both employ the formulation of the water vapor nonline continuum contribution of *Roberts et al.* [1976] to the spectrum.

The question of the accuracy of the LBL calculations is relatively straightforward for the case of CO₂, since there is no significant continuum, and good laboratory measurements do exist for values of p , T , and absorber amount close to those required for atmospheric calculations. In an important paper, *Kiehl and Ramanathan* [1983] compared the results of various band model parameterizations to the measurements of *Burch et al.* [1962], and showed that the calculated and measured frequency-integrated absorptions agreed to within 10% or better. In Figure 2 we display a plot similar to that of these authors, of the fractional error in the GFDL LBL CO₂ absorptions relative to the laboratory measurements cited above. The details of the LBL calculations are identical to those described by *Fels and Schwarzkopf* [1981]. It will be seen agreement is very good, generally to better than 5%. This is true not only for 246 K, the case shown, but also for 274 and 310 K.

Some caution is necessary here, since comparisons of frequency-integrated absorption may conceal errors in the detailed spectral data. Indeed, it is well known that for CO₂, there are important effects due to line mixing which are not accounted for by the LBL model used here. While these are of importance in applications such as remote sensing, they apparently make little difference for the calculation of fluxes and heating rates.

Although the situation with respect to the contribution of carbon dioxide seems to be relatively good, the same is not true with regard to water vapor. While it has been recognized for many years [e.g., *Bignell*, 1970] that the character of the window-region continuum is of considerable importance, it is only recently that attempts have been made to measure and assess its importance in other parts of the spectrum. For many of the models in the ICRCM study, the continuum formulation is that of *Roberts et al.* alluded to above. Based on the laboratory measure-

ments, these workers show that between 400 and 1200 cm⁻¹, there exists a contribution to the absorption coefficient (in addition to that due to local lines) of the form

$$k = C(v, T)e \quad (5)$$

where e is the water vapor partial pressure and $C(v, T)$ is a complicated function of frequency and temperature. Because of the dependence on e , this absorption is only of real importance in those parts of the atmosphere containing significant amounts of water (i.e., below 500 mbar). *Roberts et al.* claim that in the window region, the data are consistent with the p -type continuum being negligible.

The simplicity of this formulation and the accuracy with which it fits the experimental data have made this a popular way of including the continuum in radiative transfer models. It is by no means obvious, however, that this is the most accurate expression available. Based on theoretical models of line shape, and on careful analysis of the experimental data of *Burch* and co-workers, *Clough* and his collaborators [*Clough et al.*, 1989] have concluded that the continuum is of importance at all frequencies, and that it contains a significant p -type component:

$$k = C_1(v, T)p + C_2(v, T)e \quad (6)$$

The importance of the difference between these continua is seen dramatically in Figure 3, which shows water-only cooling rates for the MLS sounding computed using the two different formulations. Interestingly, the largest differences occur near 200 mbar. In that region, the larger cooling rates produced by the *Clough et al.* version are due to the inclusion of the p -type contribution absent in the *Roberts et al.* version.

The fact that tropospheric cooling rates depend so much on the details of the continuum is particularly vexing because this absorption is very difficult to establish experimentally. In part, this is because there exists no simple and universally accepted

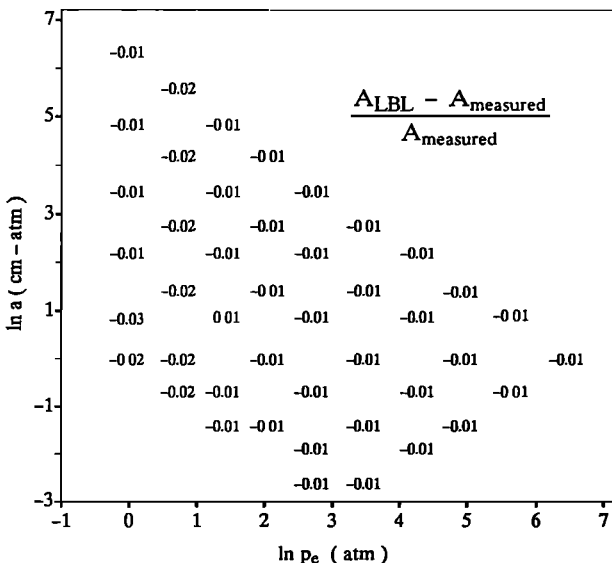


Fig. 2. Fractional differences between laboratory-observed and the GFDL line-by-line model calculated 15- μ m band absorptance as functions of absorber amount α and pressure P_e at a temperature of 246 K.

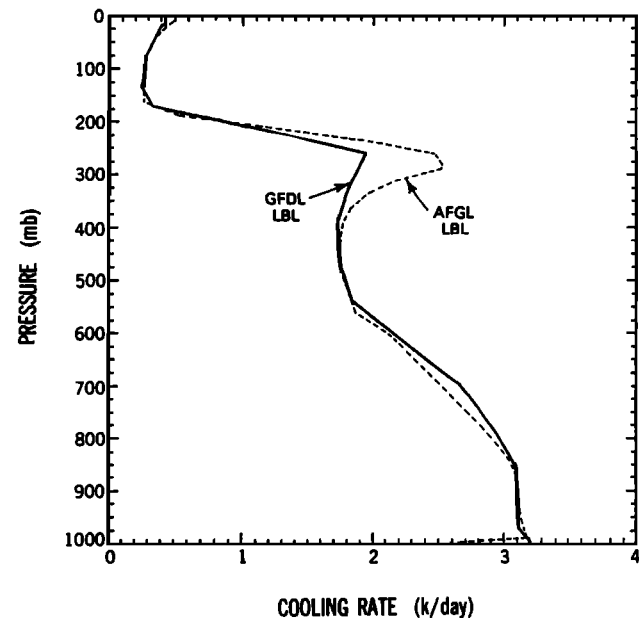


Fig. 3. A comparison of cooling rates calculated with the GFDL (solid line) and AFGL (dashed line) line-by-line models using water vapor as the only active gas. The calculations use the H₂O and temperature distributions of the mid-latitude summer atmosphere.

theory that can be used to guide laboratory measurements. This can be seen very clearly when one recognizes that the continuum is by definition any absorption not accounted for by the total contribution of all lines. Any measurement of the continuum therefore implies a specific set of assumptions about the far-wing behavior of the spectral lines. To the extent that these assumptions are arbitrary, so is the specification of the continuum.

This becomes especially important when the dependence of the continuum absorption on e and p is considered. Experimentally, this is not easy to sort out, but it can be of great practical significance, as the intercomparison shown above indicates. If the laboratory measurements are made for absorber paths and partial pressures appropriate to the relevant part of the atmosphere, they can be used with considerably more confidence than if a large extrapolation in p and e is required.

In summary, because the principal uncertainties associated with the LBL technique involve basic spectroscopic quantities common to all techniques, rather than the integrations, the LBL calculations serve as a reference to check more approximate techniques. However, their use as absolute benchmarks for atmospheric calculations is limited to those gases, such as CO₂, where calibrations with laboratory observations have been performed.

2.3. Band Models

2.3.1 Narrow band models. A common approximation for performing the frequency integration consists of dividing the spectrum into a finite number of spectral intervals that are small enough to regard B_ν in equation (1) as constant across the interval, yet wide enough to smooth out the detailed spectral features. This technique, usually called the narrow band model (NBM) technique, requires the calculation of the frequency-averaged transmissivity T_i which may be written as

$$T_i(z, z'; \mu) = \frac{1}{\Delta\nu_i} \int \exp \left(- \int_z^{z'} k_\nu Q_a \frac{dz''}{\mu} \right) d\nu \quad (7)$$

where, typically, $\Delta\nu < 100 \text{ cm}^{-1}$ and i is an index for the frequency or wave number interval. Techniques for determining T_i have been discussed in detail by Goody [1964], but some aspects of the problem bear repeating. First, note that there is no analytic solution to the problem without major assumptions concerning the variation of k_ν in $\Delta\nu$ and with p and T . A common approach to the problem is to first determine a solution T_i^* to equation (7) for the analogous homogeneous path problem with absorber amount a at p and T . That is,

$$T_i^*(a, p, T) = \frac{1}{\Delta\nu_i} \int \exp [-k_\nu(p, T)a] d\nu \quad (8)$$

After the functional form of T_i^* is found, T_i is estimated by "scaling" the inhomogeneous atmospheric path to an equivalent homogeneous one. That is,

$$T_i(z, z', \mu) \approx T_i^*(\bar{a}/\mu, \bar{p}, \bar{T}) \quad (9)$$

where \bar{a} , \bar{p} , and \bar{T} are the scaled amount of absorber, pressure, and temperature for the vertical path from z to z' .

Several different approaches are used to determine the functional dependence of T_i^* on a , p , and T . One approach involves making assumptions concerning the distributions of the line parameters S_j and f_j , which will allow T_i^* to be expressed in terms of analytical functions with adjustable parameters. The parameters for a given spectral interval are specified either from laboratory observations or by forcing agreement with spectroscopic theory in asymptotic limits. Scaling to the atmosphere is done with the use of the Curtis-Godson approximation [Goody, 1964], which defines a temperature-scaled amount of absorber at a definable mean pressure. Several different band models are discussed by Goody [1964] and applications to flux calculations have been numerous [e.g., Rodgers and Walsh, 1966; Haurwitz and Kuhn, 1974; Ellingson and Gille, 1978].

A somewhat different NBM approach transforms equation (8) to an integral over k_ν in $\Delta\nu$, and the distribution of k_ν is determined from LBL calculations [e.g., Chou and Arking, 1980; Wang and Shi, 1988]. This so-called k -distribution technique is applied to atmospheric problems with the use of a one-parameter scaling approximation. Closely related to this technique is the sum of exponentials technique as discussed by Lacis and Hansen [1974], among others. The advantages of the k -distribution technique over the analytical band model are that the actual distributions of k_ν are employed, the frequency integration is accurately performed for homogeneous paths, and the form of the expression for T_i^* allows a radiation model to be extended to include multiple scattering. The selection of scaling terms, however, is not straightforward.

Another type of NBM uses empirical functions fit to a small range of observations or calculations (e.g., LOWTRAN [Selby et al., 1976; Kneizys et al., 1988]). Although useful to some applications, this type of approach may lead to large uncertainties when the empirical functions are used beyond the range of variables for which they were intended.

The analytical models suffer in that one function cannot reasonably be applied to the spectra of one gas, let alone all gases in all spectral intervals. However, the associated errors may be reduced by a judicious selection of adjustable parameters, such as $\Delta\nu$ and the probability distribution of S_j . Nevertheless, random band model theory does not tell us how to choose $\Delta\nu$. Comparisons with line-by-line calculations have shown that intervals in the range of 5 to 20 cm^{-1} yield the best results for CO₂ and H₂O, but intervals larger than 100 cm^{-1} and smaller than 5 cm^{-1} often yield large errors. Thus the "judicious selection" of $\Delta\nu$ must be guided by line-by-line calculations or accurate laboratory data.

Application to atmospheric problems with the Curtis-Godson approximation has firmer theoretical foundations than do the one-parameter scaling approximations. Although these models yield the correct asymptotic limits, this by no means assures that they will give satisfactory results for atmospheric problems when the optical path is far from the fitted asymptotes. Modelers are often lulled into complacency by the beauty of easily calculated analytic functions. However, short of comparison with laboratory observations or line-by-line models, there is no absolute criterion for selecting the critical parameters. Nevertheless, the NBM calculations overcome the computer time limitations of the LBL technique when applied to some climate model applications (e.g., frequent one-dimensional calculations). However,

the NBMs generally require too much computer time for practical applications in two- and three-dimensional climate models.

2.3.2. Wide-band models. The third general approach to the transmission-absorption problem is the use of observations, LBL calculations, or NBM calculations to construct models of the absorption over large band widths, or even the entire spectrum. These approaches are denoted here as wide-band models (WBM). One example of this approach is the so-called emissivity approximation, which is an attempt to perform the entire spectral integration separately for each absorber. An historical account of emissivities is given by *Hottel and Sarofim* [1967], who point out that *Schack* [1924] was perhaps the first to show how data could be used to predict the emissivity. Atmospheric applications of this approach date at least to *Elsasser* [1942], and modifications and improvements are discussed by *Ramanathan* [1976]. This approach is appealing to climate studies because the integrated absorption for the active gases may be measured over a wide range of variables in the laboratory, and because the calculations may be performed rapidly on the computer. For example, *Ramanathan* [1976] and *Kiehl and Ramanathan* [1983] show good agreement of model-predicted and laboratory-observed integrated CO₂ absorptivities for the 15-μm band system. The primary difficulties with this approach are accurately accounting for the inhomogeneous path and for overlap with other active gases.

A more recent WBM approach might be called the perturbation technique. As pointed out by *Curtis* [1956] and applied by *Rodgers* [1967], it is useful to precompute the transmissivity for those constituents that do not change and are weakly dependent on temperature variations along the atmospheric path. *Fels and Schwarzkopf* [1981] extended this idea by computing the integrated absorptivities for the 15-μm band of CO₂ with an LBL integration for a standard pressure grid. Furthermore, they give the necessary matrices for extending the calculations to other pressures and temperatures. The major limitations of this approach include the necessity of large computer storage compared with the emissivity approach, the difficulty in accurately accounting for overlap with other absorbers, and the difficulty in accounting for a varying absorber concentration.

A technique related to the perturbation technique is the table look-up technique. In this approach, the pressure increments of atmospheric layers are fixed, except for perhaps the layer closest to the surface. The H₂O, CO₂, and O₃ transmissivities are precomputed for a wide range of temperature and absorber amounts in each layer. When an actual sounding is used, the data are interpolated to the model grid, the necessary absorber amounts are calculated, and the integrals are calculated through interpolation of the precomputed data. This is very similar to a computerized version of the various radiation charts. *Chou and Arking* [1980] and *Chou and Peng* [1983] have developed such a technique for H₂O and CO₂, respectively.

2.3.3. Treatment of overlapping absorption. One of the more overlooked problems in atmospheric absorption is the simultaneous absorption by two or more constituents across the same spectral interval (i.e., overlapping absorption). This is a particularly important problem for H₂O and CO₂ absorption in the 10- and 15-μm regions; for H₂O and O₃ absorption in the 9.6-μm region; and for H₂O, CH₄, and N₂O in the 7-μm region. In general, the frequency-averaged transmissivity for two gases absorbing in Δν, T_{12} , may be written as

$$T_{12} = \frac{1}{\Delta\nu_i} \int \exp(-k_{\nu_1}a_1 k_{\nu_2}a_2) d\nu \quad (10)$$

where a_1 and a_2 are the absorber amounts for the two gases. For a narrow spectral interval for which there is little correlation between the individual lines or for which there is no wave number variation in either or both gases, equation (10) may be written as

$$T_{12} = T_{11}T_{12} \quad (11)$$

Experimental studies of the appropriateness of equation (11) have been reported by *Burch et al.* [1956], *Hoover et al.* [1967], and *Tubbs et al.* [1967] for overlapping bands of several different gases. These studies have shown that if a spectral interval is broad enough to contain several lines, if the line centers are not commensurate, and if the partial pressure of the broadening gas is much greater than the partial pressures of the absorbing gases, then the average error of equation (11) is of the order of a few percent.

When the integration in equation (10) extends over an entire band area, the multiplication property expressed by equation (11) holds only if the correlation between the absorption features of the two gases is small. Different investigators express their versions of equation (10) in terms of absorptivities of the individual gases and an overlap term in the form of equation (11) for a large band area. *Burch et al.* [1956] have shown experimental results that verify this type of approach for some overlapping bands of atmospheric gases. However, the overlap correction term is not necessarily linear in the band absorptance as is assumed in climate model calculations. Overall, little evidence has been shown concerning the accuracy of these overlap approximations for all of the active atmospheric gases for either homogeneous path or atmospheric calculations.

The issue of overlapping absorption is important to climate assessment particularly when one or both of the overlapping bands have strong absorption lines as is the case between the 15-μm bands of CO₂ and the rotational band of H₂O in the 12–18 μm spectral region. *Kiehl and Ramanathan* [1982] studied the effect of this overlap on the radiative heating resulting from increased CO₂, and they showed that there is a substantial reduction in the magnitude of increase in downward flux to the surface when the overlap is included. The greatest difference occurs at tropical H₂O latitudes where there is a larger amount of H₂O. When the overlap with the continuum in the 12–18 μm region is added, there is very little increase in downward flux to the surface in the tropics from doubled CO₂ because the lower tropical atmosphere is already essentially opaque. When band overlap is included, there is a substantial increase in the tropospheric heating rates, which tends to compensate for the reduction in downward flux at the surface. Thus the degree of overlap in this spectral region affects the way the net warming is partitioned between the surface and the troposphere, but has only a weak effect on the total heating of the troposphere.

2.4. Integration Over Angle And Altitude

The integrals over angle and altitude in equation (1) generally pose less of a problem because of the relatively slow variation of the various quantities with these variables. For monochromatic radiation, the flux transmissivity (equation (2)) is simply the second exponential integral with the argument given by the integral of equation (3). Tabular values of this function are widely available, and simple, yet accurate, quadrature schemes for it are given by *Chandrasekar* [1960].

When narrow- or wide-band models are used, the integral over ν is typically performed before that over μ. Usually, the

integral over μ cannot be expressed in terms of analytic functions for the various band models. A simplification, often ascribed to Elsasser [1942], is to replace $1/\mu$ in the resulting transmission function with a constant r , called the diffusivity factor. That is,

$$T_{F\lambda}(z, z') = T_i^*(r\bar{a}, \bar{p}, \bar{T}) \quad (12)$$

This approximation is equivalent to assuming an isotropic radiation field with an intensity the same as the actual field at a zenith angle of $\cos^{-1}(1/r)$.

For monochromatic radiation, r decreases from 2 with increasing optical depth. However, most broadband and narrow-band modelers chose a constant value for r for band models and for the continuum, with 5/3 being a frequently used value. Hitchfeld and Houghton [1961] and Rodgers and Walshaw [1966] showed that this approximation yields relative errors in heating rates of about 1.5% for most atmospheric conditions. Larger errors are possible, however, with near discontinuities in temperature and moisture. For flux calculations, Ellingson and Gille [1978] reported maximum errors of the order of 0.3 W m⁻² for tropical conditions. Because the errors due to this approximation are typically an order of magnitude smaller than those due to other uncertainties, and because of the time-saving factor, most modelers chose to use this approximation.

There are actually two integrals over altitude (i.e., equations (1) and (3)). The integral over optical path in equation (3) is not difficult to evaluate because the absorption coefficient and absorber density are usually continuous and relatively slowly varying functions of altitude, at least for clear-sky conditions. This integral does not appear explicitly in terms of κ_ν for the band models. Instead, these models yield similar integrals in terms of band model parameters chosen on an ad-hoc basis or to give correct asymptotic results (i.e., the Curtis-Godson approximation). These approximations may lead to transmittance errors, as discussed by Goody [1964], which are particularly large when most of the absorbing material is at low pressure (e.g., O₃). It is these scaling approximations, not the evaluation of the optical path integral, that is another source of discrepancy with line-by-line calculations when these models are applied to the atmosphere.

The evaluation of the integral over altitude in equation (1) is governed primarily by the altitude variation of $T_{F\lambda}$. In opaque regions of the spectrum, $T_{F\lambda}$ may vary between 1 and 10⁻⁴ across a few tens of meters, in some regions of the atmosphere. Large errors will result if too coarse a vertical resolution is used in regions where there are also large variations in B_ν . However, too fine a resolution becomes computationally prohibitive, and may not be necessary for a particular application. Thus modelers make compromises on the vertical resolution that depend on the application, the width of the spectral intervals, the band model used in the model and the particular integral over altitude (i.e., equation (1) or its integrated by parts version). The choices are usually made on the basis of trial and error, if made at all.

There is no set of established criteria on how to choose the proper vertical resolution or type of quadrature for a given problem. For the ICRCCM soundings, Ellingson found that a two-point Gaussian quadrature per sounding layer (the order of 1 km) was more than sufficient for 0.1% accuracy in flux calculations with his NBM. This type of resolution is overkill for some problems, but it is not sufficient when there is detailed vertical structure to the temperature and moisture distributions.

An alternative to testing models with high-order quadratures is testing a chosen scheme with analytic functions. For example,

the actual variation of the integrand between successive model levels might be approximated by assuming the Planck function to vary linearly in pressure while the transmittance varies as the square root of pressure. These assumptions lead to an analytic solution to the integral in terms of a few adjustable parameters. A model's numerical scheme can be tested by comparing the numerical and analytic solutions over a wide range of the parameters.

A trivial but important result to check is a model's output for an isothermal atmosphere, for which the upward flux is constant with altitude, and the downward flux may be determined from the Planck function and the transmittance from a given level to space. Although the importance of these type tests are known to many modelers, it appears that they are not always done in practice, as we shall see later.

2.5. Summary of Model Approaches

Each of the approaches (LBL, NBM, and WBM) has some usefulness to climate modeling. The LBL calculations are useful for checking the accuracy of NBM and WBM frequency integrations for homogeneous paths relative to the basic spectroscopic data. In addition, they allow for checks on the approximations made for the integrations over atmospheric path. The NBM calculations are particularly useful for one-dimensional studies requiring high relative accuracy. Furthermore, the absolute accuracy of the calculations may be checked by comparing calculations with observations in narrow spectral intervals such as those that are available from space platforms or instrumented aircraft. Also, the NBM calculations may be used to calibrate the WBM calculations over a larger range of variables than might easily be checked with LBL calculations. The WBM calculations are best suited for the rapid calculations necessary for many climate studies, particularly those involving general circulation models.

There is no simple way to quantify the magnitudes of the errors associated with the different approximations because they are model dependent. As an example, however, we reproduce in Table 2 the results of Morcrette [1984], who studied some of these effects with a particular narrow band model. Beginning with his unaltered model, different simplifications were sequentially implemented. The change in absorption listed in Table 2 applies to the single simplification indicated, but the model at each stage includes all of the changes higher on the list. The main lesson from Table 2 is that the impact of simplifications can vary in sign and magnitude. Consequently, it is possible to incorporate a combination of changes with the net result that the calculations do not differ greatly from the much more detailed model. However, because the changes vary from profile to profile, the various simplifications may not be appropriate for routine use. Furthermore, these results tell us that there could be large discrepancies between similar models due only to numerical approximations.

3. ICRCCM TEST CASES

Clear-sky calculations have been performed for 55 separate sets of input conditions with the aims of determining the range of flux and heating rate variations among models and testing model sensitivity to individual gas concentrations, temperature, overlap among gases and continua effects. The cases included isothermal atmospheres with CO₂ alone (300 and 600 ppmv) and H₂O alone, the five AFGL reference atmospheres [McClatchey et al., 1971] with all absorbing gases active, AFGL atmospheres with CO₂ only (300 and 600 ppmv), an AFGL atmosphere with all absorbing gases active with $\pm 25\%$ perturbations in the H₂O content,

TABLE 2. Impact of Simplifying Assumptions on the Results of a Long-Wave Radiation Narrow-Band Model

Simplification	Impact on Atmospheric Absorption	Change in Atmospheric Absorption, W m^{-2}	
		Subarctic Winter	Tropical
N layers 40 \rightarrow 10	decrease	-4.0	-5.0
$L = 8 \rightarrow L = 2^*$	decrease	-0.5	-1.5
$G2 \rightarrow G2T^{**}$	decrease	-0.8	-4.0
$T, q \rightarrow T, \bar{q} \dagger$	increase	+4.0	+5.0
Voigt \rightarrow Lorentz lines	decrease	-2.5	-4.5
\rightarrow Strong line regime	increase	+6.0	+7.0
Neglect N_2O and CH_4	decrease	-4.5	-5.0
CO_2 15 μm , O_3 9.6 $\mu\text{m} \ddagger$	decrease	-2.0	-5.0
Reduce number of spectral intervals	increase	Depends on initial width of spectral intervals	

From Morcrette [1984].

*Decreasing the order of numerical quadrature used for vertical integration.

**Two-point Gaussian quadrature for nearby layers, trapezoidal rule for distant layers.

\dagger Using averaged values within layers.

\ddagger Limiting CO_2 to 500–800 cm^{-1} and O_3 to 970–1110 cm^{-1} .

O_3 only (normal and perturbed), H_2O only (normal and perturbed; with and without continuum absorption), CH_4 and N_2O alone; and two atmospheric profiles for which flux measurements were available.

Six different sets of radiation calculations were performed in the presence of complete cloud cover with the aim of testing the sensitivity to the drop size distribution, the location of the cloud top and the cloud liquid water content. The clouds were specified to be 1 km thick, and the calculations were performed with cloud tops of 2 and 13 km. Two different cloud droplet size distributions were selected from the work of Stephens [1979]: a size distribution with small droplets (CS) and a size distribution with large droplets (CL). These correspond to Stephens' Sc I (CS) and Cb (CL) distributions which have effective radii of 5.25 and 31 μm , respectively. The liquid water content (LWC) was specified to be either 10 g m^{-2} (nonblack cloud for both CS and CL) or 200 g m^{-2} (near-black cloud for CL). The calculations were performed with one cloud layer present at a time with 300 ppmv CO_2 for the temperature, H_2O , and O_3 distributions given by the MLS atmosphere.

The complete list of cases is given in Table 3 along with the case numbers and a summary description (Table 4). Tables 5–9 list the atmospheric parameter data used with the ICRCM versions of the AFGL atmospheres. A comprehensive list of instructions for those wishing to do the calculations is available from the authors. Tables 10 and 11 provide summary information on the results of each case.

4. RESULTS

Each test case has not been thoroughly examined. Instead, the analysis has concentrated on some of the MLS atmosphere cases highlighted in the paper by Luther et al. [1988]. The primary purpose of the analysis is to determine some of the causes for the clear-sky differences found in that study and to summarize the cloudy-sky results. Our clear-sky analysis has been done with the

use of extensive information concerning each model obtained from responses to questionnaires distributed to the participants. The calculations discussed herein as 1988 results consist of all the calculations received as of April 1, 1988 (i.e., none of the withdrawn calculations are included in the 1988 sample).

4.1. Clear-Sky Study

4.1.1. *Features of the clear-sky results.* As an indication of the range of agreement between model flux calculations and the manner by which these have changed over the course of ICRCM, we show in Figure 4 a comparison of the 1984 (open) and 1988 (shaded) distributions of downward fluxes at the surface relative to line-by-line calculations. The LBL calculations are from the Fels-Schwarzkopf (GFDL) model, and the MLS profile with all of the constituents (i.e., H_2O , O_3 , and 300 ppmv CO_2) was used as input to all models. For this case, the 1988 data show nine more non-LBL models that agree to within $\pm 2\%$ of the GFDL LBL results, seven of these being from new participants. Of the 22 climate model type calculations for this case, 13 are within the $\pm 2\%$ range, and all but one fall within the $\pm 6\%$ range. On a percentage basis, 67% of the 1988 non-LBL model results agree to within $\pm 2\%$ of the LBL results as compared with 58% in 1984. Similar results hold for the net flux comparisons at the tropopause and the upward flux at the top of the atmosphere for this atmospheric profile.

The increase in the fraction of models agreeing closer with the LBL results also holds for the change of the net flux between the surface and tropopause (13 km), denoted ΔF_{net} , as illustrated in Figure 5. The 1988 data find more than twice the number of models agreeing with the LBL results to within $\pm 2\%$ than the 1984 data. About 82% of the 1988 and 75% of the 1984 model data agree with the LBL results when the range for agreement is increased to $\pm 6\%$, or a rate of temperature change of about $\pm 0.1 \text{ K/d}$. However, only 60% of the climate model type calculations fall within this $\pm 6\%$ range. It should be noted that comparisons of vertical profiles of flux divergence have not been examined in detail, but our experience with the 1984 data suggests that much larger differences than those noted above will be found in some layers.

Although Figures 4 and 5 give some confidence in the general ability of the less detailed models to reproduce the gross features of the line-by-line results, this confidence is shaken somewhat when we examine the results when H_2O is the only absorbing gas as shown in Figure 6. When only the local lines of H_2O are included in the downward flux calculations, more than half of the results are outside of the $\pm 2\%$ range, which was also seen in the 1984 data (not shown). The continuum masks many of the very large positive differences, but it also amplifies many of the large negative ones. In general, the effect of the continuum and the overlap of different species tends to mask many of the large differences between absorption parameterizations of individual gases. Although this masking reduces the range of flux values expected from absorption differences alone, it also prohibits extending the range of agreement of this study to significantly different atmospheric conditions.

One of the major areas of study for ICRCM was the sensitivity to changes in the concentration of the major absorbers, particularly CO_2 . An important quantity calculated in CO_2 doubling studies is the change in the net flux at the tropopause as CO_2 doubles, denoted as δF_{net} . Figure 7 shows the distribution of δF_{net}

TABLE 3. Summary of ICRCM Long-Wave Clear-Sky Cases

Case	Description
1	Isothermal atmosphere 200 K, CO ₂ only 300 ppmv
2	Isothermal atmosphere 200 K, CO ₂ only 600 ppmv
3	Isothermal atmosphere 250 K, CO ₂ only 300 ppmv
4	Isothermal atmosphere 250 K, CO ₂ only 600 ppmv
5	Isothermal atmosphere 300 K, CO ₂ only 300 ppmv
6	Isothermal atmosphere 300 K, CO ₂ only 600 ppmv
7	CO ₂ only 300 ppmv, tropical atmosphere
8	CO ₂ only 600 ppmv, tropical atmosphere
9	CO ₂ only 300 ppmv, mid-latitude summer
10	CO ₂ only 600 ppmv, mid-latitude summer
11	CO ₂ only 300 ppmv, mid-latitude winter
12	CO ₂ only 600 ppmv, mid-latitude winter
13	CO ₂ only 300 ppmv, subarctic summer
14	CO ₂ only 600 ppmv, subarctic summer
15	CO ₂ only 300 ppmv, subarctic winter
16	CO ₂ only 600 ppmv, subarctic winter
17	H ₂ O only, 0.75 * H ₂ O concentration with continuum, mid-latitude summer
18	H ₂ O only, 0.75 * H ₂ O concentration without continuum, mid-latitude summer
19	H ₂ O only, 1.00 * H ₂ O concentration with continuum, mid-latitude summer
20	H ₂ O only, 1.00 * H ₂ O concentration without continuum, mid-latitude summer
21	H ₂ O only, 1.25 * H ₂ O concentration with continuum, mid-latitude summer
22	H ₂ O only, 1.25 * H ₂ O concentration without continuum, mid-latitude summer
23	O ₃ only, mid-latitude summer: (a) 14 μ m band, (b) 9.6 μ m band, (c) 9.6 and 14 μ m band
24	O ₃ only, scaled concentrations, mid-latitude summer
24(a)	Decrease O ₃ above 13 km by 25% (9.6 μ m band)
24(b)	Decrease O ₃ above 13 km by 25% (9.6 and 14 μ m bands)
24(c)	Increase O ₃ below 13 km by 25% (9.6 μ m band)
24(d)	Increase O ₃ below 13 km by 25% (9.6 and 14 μ m bands)
25	All constituents (CO ₂ , H ₂ O, O ₃), 300 ppmv CO ₂ , tropical
26	All constituents (CO ₂ , H ₂ O, O ₃), 600 ppmv CO ₂ , tropical
27	All constituents (CO ₂ , H ₂ O, O ₃), 300 ppmv CO ₂ , mid-latitude summer
28	All constituents (CO ₂ , H ₂ O, O ₃), 600 ppmv CO ₂ , mid-latitude summer
29	All constituents (CO ₂ , H ₂ O, O ₃), 300 ppmv CO ₂ , mid-latitude winter
30	All constituents (CO ₂ , H ₂ O, O ₃), 600 ppmv CO ₂ , mid-latitude winter
31	All constituents (CO ₂ , H ₂ O, O ₃), 300 ppmv CO ₂ , subarctic summer
32	All constituents (CO ₂ , H ₂ O, O ₃), 600 ppmv CO ₂ , subarctic summer
33	All constituents (CO ₂ , H ₂ O, O ₃), 300 ppmv CO ₂ , subarctic winter
34	All constituents (CO ₂ , H ₂ O, O ₃), 600 ppmv CO ₂ , subarctic winter
35	All constituents, 300 ppmv CO ₂ , without H ₂ O continuum, mid-latitude summer
36	All constituents, 600 ppmv CO ₂ , without H ₂ O continuum, mid-latitude summer
37	Trace gases CH ₄ , 1.75 ppmv and N ₂ O, 0.28 ppmv, mid-latitude summer: (a) CH ₄ , (b) N ₂ O, (c) N ₂ O 4.5 μ m band, (d) N ₂ O 17 μ m band, (e) N ₂ O 7.8 and 8.6 μ m bands, (f) N ₂ O 4.5, 7.8, 8.6 and 17 μ m bands and (g) CH ₄ and N ₂ O
38	Isothermal atmosphere 200 K, H ₂ O only, 0.01 g/g, with continuum
39	Isothermal atmosphere 200 K, H ₂ O only, 0.01 g/g, without continuum
40	Isothermal atmosphere 250 K, H ₂ O only, 0.01 g/g, with continuum
41	Isothermal atmosphere 250 K, H ₂ O only, 0.01 g/g, without continuum
42	Isothermal atmosphere 300 K, H ₂ O only, 0.01 g/g, with continuum
43	Isothermal atmosphere 300 K, H ₂ O only, 0.01 g/g, without continuum
44(a)	H ₂ O e-type continuum only, mid-latitude summer
44(b)	H ₂ O e-type e-type and p-type continuum only, mid-latitude summer
45	H ₂ O p-type continuum only, mid-latitude summer
46(a)	H ₂ O e-type continuum only, tropical
46(b)	H ₂ O e-type and p-type continuum only, tropical
47	H ₂ O p-type continuum only, tropical
48	Isothermal atmosphere 250 K, CO ₂ only 300 ppmv, without temperature correction
49	Isothermal atmosphere 250 K, CO ₂ only 600 ppmv, without temperature correction
50	Isothermal atmosphere 300 K, CO ₂ only 300 ppmv, without temperature correction
51	Isothermal atmosphere 300 K, CO ₂ only 600 ppmv, without temperature correction
52	All constituents (CO ₂ , H ₂ O, O ₃), 300 ppmv CO ₂ , mid-latitude summer, 0.75 x H ₂ O concentration with continuum
53	All constituents (CO ₂ , H ₂ O, O ₃), 300 ppmv CO ₂ , mid-latitude summer, 0.75 x H ₂ O concentration without continuum
54	All constituents (CO ₂ , H ₂ O, O ₃), 300 ppmv CO ₂ , mid-latitude summer, 1.25 x H ₂ O concentration with continuum
55	All constituents (CO ₂ , H ₂ O, O ₃), 300 ppmv CO ₂ , mid-latitude summer, 1.25 x H ₂ O concentration without continuum

TABLE 4. Summary of ICRCM Long-Wave Cloudy-Sky Cases

Case	Description
1	All gases, mid-latitude summer, CS cloud, cloud top 13 kk liquid water 10 g m ⁻² , 300 ppmv
2	All gases, mid-latitude summer, CS cloud, cloud top 2 km, liquid water 10 g m ⁻² , 300 ppmv CO ₂
3	All gases, mid-latitude summer, CI cloud, cloud top 13 km, liquid water 10 g m ⁻² , 300 ppmv CO ₂
4	All gases, mid-latitude summer, CI cloud top 13 km, liquid water 200 g m ⁻² , 300 ppmv CO ₂
5	All gases, mid-latitude summer, CI cloud, cloud top 2 km, liquid water 10 g m ⁻² , 300 ppmv CO ₂
6	All gases, mid-latitude summer, CI cloud, cloud top 2 km, liquid water 200 g m ⁻² , 300 ppmv CO ₂

TABLE 5. Data for the Tropical Atmosphere

Height, km	Pressure, mbar	Temperature, Kelvins	H ₂ O Density, g m ⁻³	O ₃ Density, g m ⁻³
0	1.013E+03	300.0	1.90E+01	5.6E-05
1	9.040E+02	294.1	1.30E+01	5.6E-05
2	8.050E+02	288.4	9.29E+00	5.4E-05
3	7.150E+02	283.6	4.70E+00	5.1E-05
4	6.330E+02	277.4	2.66E+00	4.7E-05
5	5.590E+02	270.7	1.53E+00	4.5E-05
6	4.920E+02	264.0	8.60E-01	4.3E-05
7	4.320E+02	257.3	4.71E-01	4.1E-05
8	3.780E+02	250.6	2.50E-01	3.9E-05
9	3.290E+02	243.8	1.21E-01	3.9E-05
10	2.860E+02	237.2	4.90E-02	3.9E-05
11	2.470E+02	230.4	1.79E-02	4.1E-05
12	2.130E+02	223.8	6.08E-03	4.3E-05
13	1.820E+02	217.0	1.79E-03	4.5E-05
14	1.560E+02	210.4	9.86E-04	4.5E-05
15	1.320E+02	203.6	7.57E-04	4.7E-05
16	1.110E+02	196.8	6.37E-04	4.7E-05
17	9.370E+01	195.6	5.42E-04	6.9E-05
18	7.890E+01	199.5	4.48E-04	9.0E-05
19	6.660E+01	203.6	3.70E-04	1.4E-04
20	5.650E+01	207.6	3.08E-04	1.9E-04
21	4.800E+01	211.5	2.57E-04	2.4E-04
22	4.090E+01	214.6	2.16E-04	2.8E-04
23	3.500E+01	216.9	1.83E-04	3.2E-04
24	3.000E+01	219.1	1.55E-04	3.4E-04
25	2.570E+01	221.3	1.31E-04	3.4E-04
30	1.220E+01	232.3	5.95E-05	2.4E-04
35	6.000E+00	243.3	2.79E-05	9.2E-05
40	3.050E+00	254.3	1.36E-05	4.1E-05
45	1.590E+00	264.9	6.80E-06	1.3E-05
50	8.540E-01	270.0	3.58E-06	4.3E-06
70	5.790E-02	219.5	2.99E-07	8.6E-08
103	3.000E-04	209.9	1.62E-09	4.3E-11

Read, for example, 1.013E+3 as 1.013×10^3

relative to the LBL calculations clear-sky MLS conditions. The LBL models agree on this result to about $\pm 1\%$ of 5.6 W m^{-2} . However, the various band model results differ by up to 50% of this value. Of the 17 codes actually used in climate models, six fall within $\pm 5\%$ of the LBL results, and one differs by more than 25%. The close agreement with LBL results for some of these models is not surprising because they have been tuned to LBL calculations.

4.1.2. Examination of the clear-sky calculations. Our choice of model calculations to study is based on their sensitivity to model and atmospheric variables. The downward flux at the surface ($F \downarrow$) has been chosen for flux considerations because it is more sensitive than the upward fluxes at the tropopause and

TABLE 6. Data for the Mid-Latitude Summer Atmosphere

Height, km	Pressure, mbar	Temperature, Kelvins	H ₂ O Density, g m ⁻³	O ₃ Density, g m ⁻³
0	1.013E+03	294.0	1.40E+01	6.0E-05
1	9.020E+02	290.0	9.30E+00	6.0E-05
2	8.020E+02	285.0	5.85E+00	6.0E-05
3	7.100E+02	279.0	3.43E+00	6.2E-05
4	6.280E+02	273.0	1.89E+00	6.4E-05
5	5.540E+02	267.1	1.00E+00	6.6E-05
6	4.870E+02	261.0	6.09E-01	6.9E-05
7	4.260E+02	254.7	3.71E-01	7.5E-05
8	3.720E+02	248.2	2.10E-01	7.9E-05
9	3.240E+02	241.7	1.18E-01	8.6E-05
10	2.810E+02	235.2	6.43E-02	9.0E-05
11	2.430E+02	228.8	2.19E-02	1.1E-04
12	2.090E+02	222.3	6.46E-03	1.2E-04
13	1.790E+02	216.9	1.66E-03	1.5E-04
14	1.530E+02	215.8	9.95E-04	1.8E-04
15	1.300E+02	215.8	8.40E-04	1.9E-04
16	1.100E+02	215.8	7.10E-04	2.1E-04
17	9.500E+01	215.8	6.14E-04	2.4E-04
18	8.120E+01	216.0	5.24E-04	2.8E-04
19	6.950E+01	217.0	4.46E-04	3.2E-04
20	5.950E+01	218.2	3.80E-04	3.4E-04
21	5.100E+01	219.4	3.24E-04	3.6E-04
22	4.370E+01	220.6	2.76E-04	3.6E-04
23	3.760E+01	221.8	2.36E-04	3.4E-04
24	3.220E+01	223.0	2.01E-04	3.2E-04
25	2.770E+01	224.2	1.72E-04	3.0E-04
30	1.320E+01	234.2	7.85E-05	2.0E-04
35	6.520E+00	245.3	3.70E-05	9.2E-05
40	3.330E+00	257.5	1.80E-05	4.1E-05
45	1.760E+00	269.7	9.09E-06	1.3E-05
50	9.510E-01	276.2	4.80E-06	4.3E-06
70	6.710E-02	219.1	4.27E-07	8.6E-08
104	3.000E-04	209.9	1.99E-09	4.3E-11

Read, for example, 1.013E+3 as 1.013×10^3

the top of the atmosphere. For the MLS atmosphere, 13 of 36 model calculations of $F \downarrow$ differed from the average LBL result by more than 6 W m^{-2} (about 2%). However, only nine of the 39 differed from the average LBL calculation of the upward flux at the top of the atmosphere ($F \uparrow$) by more than 6 W m^{-2} (also about 2%), and only six of those were among the 13 models that produced the large differences at the surface. In order to identify 12 of the 13 models that disagreed with LBL $F \downarrow$ values by more than 2%, it was necessary to test the $F \uparrow$ values at the 1 W m^{-2} level. This also misidentified 16 of the models that agree to within 2% at the surface. However, of the 23 models that agreed within 2% of the LBL results at the surface, 20 agree to within 2% at the top. Thus comparisons between downward flux calculations at the surface appears to be a stronger test of the models' ability to calculate fluxes than are comparisons of upward fluxes. To test models for calculating heating rates, we have compared calculations of ΔF_{net} , the change of the net flux between the surface and the tropopause (13 km).

Attributing causes for the disagreements between the various models is difficult as the previously mentioned results of Morcrette illustrate. However, we have attempted to isolate some of the causes by examining common features among the models. As a first attempt, we have examined the calculations for H₂O and CO₂ separately as a function of the generic techniques used to perform the frequency integration. Specifically we divided the narrow-band and broadband calculations into the categories as listed in Table 12. Note that some models use a

TABLE 7. Data for the Mid-Latitude Winter Atmosphere

Height, km	Pressure, mbar	Temperature, Kelvins	H ₂ O Density, g m ⁻³	O ₃ Density, g m ⁻³
0	1.018E+03	272.2	3.50E+00	6.0E-05
1	8.973E+02	268.7	2.50E+00	5.4E-05
2	7.897E+02	265.2	1.80E+00	4.9E-05
3	6.938E+02	261.2	1.16E+00	4.9E-05
4	6.081E+02	255.7	6.90E-01	4.9E-05
5	5.313E+02	249.6	3.78E-01	5.8E-05
6	4.627E+02	243.6	1.89E-01	6.4E-05
7	4.016E+02	237.6	8.57E-02	7.7E-05
8	3.473E+02	231.6	3.50E-02	9.0E-05
9	2.992E+02	225.6	1.60E-02	1.2E-04
10	2.568E+02	220.6	7.50E-03	1.6E-04
11	2.199E+02	219.2	4.44E-03	2.1E-04
12	1.882E+02	218.7	2.72E-03	2.6E-04
13	1.610E+02	218.2	1.72E-03	3.0E-04
14	1.378E+02	217.7	1.13E-03	3.2E-04
15	1.178E+02	217.2	7.64E-04	3.4E-04
16	1.007E+02	216.7	6.48E-04	3.6E-04
17	8.610E+01	216.2	5.55E-04	3.9E-04
18	7.350E+01	215.7	4.75E-04	4.1E-04
19	6.280E+01	215.4	4.06E-04	4.3E-04
20	5.370E+01	215.2	3.04E-04	4.5E-04
21	4.580E+01	215.2	2.97E-04	4.3E-04
22	3.910E+01	215.2	2.53E-04	4.3E-04
23	3.340E+01	215.2	2.16E-04	3.9E-04
24	2.860E+01	215.2	1.85E-04	3.6E-04
25	2.430E+01	215.4	1.57E-04	3.4E-04
30	1.110E+01	217.3	7.12E-05	1.9E-04
35	5.180E+00	227.9	3.17E-05	9.2E-05
40	2.530E+00	244.0	1.45E-05	4.1E-05
45	1.290E+00	258.9	6.94E-06	1.3E-05
50	6.820E-01	265.6	3.58E-06	4.3E-06
70	4.670E-02	230.9	2.82E-07	8.6E-08
103	3.000E-04	210.1	1.99E-09	4.3E-11

Read, for example, 1.013E+3 as 1.013×10^3

narrow-band technique for H₂O but a wide-band model for the CO₂ calculations.

The effects of different parameterizations of O₃ are not discussed because our analysis showed little effect of these on the studied terms. However, these parameterizations will likely show large differences in stratospheric absorption and emission. The analysis of those effects are left to a later study.

Several sets of the calculations in which water vapor was the only active gas were examined in order to identify the the effects of different treatments of the spectral lines and the continuum. An important feature of the results shown in Figures 8 through 11 is that there are several NBMs and a few WBMs that are consistently within $\pm 5\%$ of the range of the LBL flux results for the combined effects of the lines and the continuum and for the effects of the lines alone. However, 5% agreement in the change in $F \downarrow$ at the surface as the continuum is added is limited to a very small number of models. It is quite clear that no model can be trusted to duplicate the LBL results.

For the NBMs in category 3, the spread between the models decreases when the continuum is added, whereas the spread increases or remains nearly unchanged for the category 4 NBMs and WBMs. With one exception, the continuum has a smaller effect on the wider band results than on those in categories 2 and 3. We suspect that the differences in the continuum sensitivities between the categories may be related to the treatment of the line and continuum overlap (i.e., the averaging of continuum coefficients over wide intervals) and to the application of the band models to the lines in the wide intervals.

TABLE 8. Data for the Subarctic Summer Atmosphere

Height, km	Pressure, mbar	Temperature, Kelvins	H ₂ O Density, g m ⁻³	O ₃ Density, g m ⁻³
0	1.010E+03	287.0	9.10E+00	4.9E-05
1	8.960E+02	281.7	6.00E+00	5.4E-05
2	7.929E+02	276.4	4.20E+00	5.6E-05
3	7.000E+02	271.1	2.69E+00	5.8E-05
4	6.160E+02	265.7	1.65E+00	6.0E-05
5	5.410E+02	259.8	9.73E-01	6.4E-05
6	4.730E+02	252.8	5.43E-01	7.1E-05
7	4.130E+02	245.8	2.90E-01	7.5E-05
8	3.590E+02	238.8	1.30E-01	7.9E-05
9	3.107E+02	231.8	4.18E-02	1.1E-04
10	2.677E+02	225.6	1.75E-02	1.3E-04
11	2.300E+02	225.0	8.56E-03	1.8E-04
12	1.977E+02	225.0	4.20E-03	2.1E-04
13	1.700E+02	225.0	2.06E-03	2.6E-04
14	1.460E+02	225.0	1.02E-03	2.8E-04
15	1.250E+02	225.0	7.77E-04	3.2E-04
16	1.080E+02	225.0	6.69E-04	3.4E-04
17	9.280E+01	225.0	5.75E-04	3.9E-04
18	7.980E+01	225.0	4.94E-04	4.1E-04
19	6.860E+01	225.0	4.25E-04	4.1E-04
20	5.890E+01	225.0	3.65E-04	3.9E-04
21	5.070E+01	225.0	3.14E-04	3.6E-04
22	4.360E+01	225.1	2.70E-04	3.2E-04
23	3.750E+01	225.5	2.32E-04	3.0E-04
24	3.227E+01	226.6	1.98E-04	2.8E-04
25	2.780E+01	227.9	1.70E-04	2.6E-04
30	1.340E+01	234.9	7.95E-05	1.4E-04
35	6.610E+00	247.2	3.73E-05	9.2E-05
40	3.400E+00	262.3	1.81E-05	4.1E-05
45	1.810E+00	274.1	9.20E-06	1.3E-05
50	9.870E-01	276.9	4.97E-06	4.3E-06
69	7.070E-02	216.8	4.55E-07	8.6E-08
104	3.000E-04	209.4	2.00E-09	4.3E-11

Read, for example, 1.013E+3 as 1.013×10^3

Since most of the NBMs in categories 2 to 4 assume random line positions, and since the distribution of line intensities is not homogeneous across the spectrum, models with smaller $\Delta\nu$ tend to have more spectral gaps which results in a higher transmittance across the spectrum. Those models are thus more sensitive to changes in opacity caused by either the addition of absorbing material or by adding the continuum (e.g., compare categories 2, 3, and 4 in Figures 8a and 8b). The results shown in Figure 9b indicate that the optimal width of band model spectral intervals for water vapor, although not well defined, is probably greater than 5 but less than 50 cm⁻¹.

Many similarities to the water vapor calculations are seen in the categorical distributions of flux and flux sensitivities to CO₂ concentrations shown in Figures 12 and 13. Overall, there is at least one model in each category that falls within $\pm 5\%$ of the LBL results for $F \downarrow$ at the surface for 300 ppmv alone and for the change of the net flux at the tropopause (δF_{net}) as CO₂ is doubled from 300 ppmv (Figures 12c and 13c). For the most part, the large spread of the net flux at the tropopause (F_{net}) (Figures 12b and 13b) tends to be rather systematic when the CO₂ concentration changes, as the spread of δF_{net} is much smaller than the differences between the various models. Thus the models will yield roughly the same radiative forcing, but radiation budgets will be different from model to model.

There is, however, a disturbingly large spread among model results for CO₂ in the various categories. A small portion of it is in part due to some models neglecting the effects of the 4.3 and 10

TABLE 9. Data for the Subarctic Winter Atmosphere

Height, km	Pressure, mbar	Temperature, Kelvins	H ₂ O Density, g m ⁻³	O ₃ Density, g m ⁻³
0	1.013E+03	257.1	1.20E+00	4.1E-05
1	8.878E+02	259.1	1.20E+00	4.1E-05
2	7.775E+02	256.4	1.03E+00	4.1E-05
3	6.798E+02	252.2	7.47E-01	4.3E-05
4	5.932E+02	246.8	4.59E-01	4.5E-05
5	5.158E+02	240.6	2.34E-01	4.7E-05
6	4.467E+02	233.9	9.78E-02	4.9E-05
7	3.853E+02	227.1	3.29E-02	7.1E-05
8	3.308E+02	220.4	1.32E-02	9.0E-05
9	2.829E+02	217.1	8.37E-03	1.6E-04
10	2.418E+02	217.1	5.51E-03	2.4E-04
11	2.067E+02	217.1	3.79E-03	3.2E-04
12	1.766E+02	217.1	2.58E-03	4.3E-04
13	1.510E+02	217.1	1.67E-03	4.7E-04
14	1.291E+02	217.1	1.10E-03	4.9E-04
15	1.103E+02	217.0	7.33E-04	5.6E-04
16	9.431E+01	216.7	6.06E-04	6.2E-04
17	8.058E+01	216.1	5.20E-04	6.2E-04
18	6.882E+01	215.5	4.45E-04	6.2E-04
19	5.875E+01	214.9	3.81E-04	6.0E-04
20	5.014E+01	214.3	3.26E-04	5.6E-04
21	4.277E+01	213.7	2.79E-04	5.1E-04
22	3.647E+01	213.1	2.38E-04	4.7E-04
23	3.109E+01	212.5	2.04E-04	4.3E-04
24	2.649E+01	212.0	1.74E-04	3.6E-04
25	2.256E+01	211.9	1.48E-04	3.2E-04
30	1.020E+01	216.6	6.56E-05	1.5E-04
35	4.701E+00	223.1	2.94E-05	9.2E-05
40	2.243E+00	235.3	1.33E-05	4.1E-05
45	1.113E+00	247.9	6.26E-06	1.3E-05
50	5.719E-01	258.9	3.08E-06	4.3E-06
70	4.016E-02	245.4	2.28E-07	8.6E-08
103	3.000E-04	209.9	1.99E-09	4.3E-11

Read, for example, 1.013E+3 as 1.013×10^3

μm bands, the magnitude of which is illustrated by the distance between the data points for NBM category 2 in Figure 12. In general, the spread of δF_{net} tends to be smaller for the NBMs than for the WBMs, which leads us to suspect the validity of some of the wide-band parameterizations of categories 3 to 5. However, the categorical distributions alone for CO₂ and H₂O give little insight as to the cause of the spread between model results.

In an attempt to explain the large range of model results seen in the different generic models, the participants' questionnaires were used to test for linkage between the model results and type of integral evaluated, the sources of spectral line and continuum data, the type of scaling approximation and tests of the accuracy of the techniques used to perform the integral over altitude. In performing the search, we decided to regroup the models according the spectral resolution used to perform the frequency integration for CO₂. This has the practical effect of associating the three models marked with diamonds in Figures 8 and 9 in category 4 with wide-band models. The various numerical categories are not used after this point.

Shown in Figure 14 is the distribution of model calculations of $F \downarrow$ as a function of the sources of model H₂O continua and spectral lines (for those models for which both references were available). Most of the NBMs and LBLs use spectral line data circa 1978 or later and the *Robert et al.*'s [1976] continuum data, whereas the WBMs use a larger variety of line and continua data. Two of the WBMs showing the largest differences with the LBL results use either no continuum, or a combination of two different continuum data sets. However, a model using no continuum, but based on the same spectral line data as a model using the *Bignell* [1970] data, agree well with each other. Similarly, the source of spectral line data does not appear to play a major role in the disagreements between models using the same continuum data.

TABLE 10. Summary of Results for the Long-Wave Clear-Sky Study

Case	Statistic	Surface			Tropopause			Top		
		Up	Down	Net	Up	Down	Net	Up	Dnet1	Dnet2
1	Average	90.72	14.47	76.22	90.73	8.22	82.47	90.75	6.24	8.28
	Std. Dev.	0.24	1.61	1.69	0.32	1.04	1.03	0.35	1.30	1.06
	Median	90.72	14.20	76.50	90.72	7.98	82.76	90.72	6.15	8.01
	Range	1.56	5.86	5.99	2.02	4.85	4.14	2.62	5.78	4.88
	Number	33	35	34	32	34	34	34	34	34
2	Average	90.76	15.64	75.08	90.78	9.51	81.20	90.80	6.12	9.60
	Std. Dev.	0.15	1.62	1.62	0.18	1.12	1.15	0.25	1.02	1.12
	Median	90.72	15.35	75.50	90.72	9.16	81.61	90.72	6.00	9.34
	Range	0.78	6.20	6.19	0.87	4.56	4.56	1.50	4.04	4.56
	Number	32	34	33	31	33	33	33	33	33
3	Average	221.41	41.81	179.61	221.42	24.27	197.09	221.47	17.48	24.38
	Std. Dev.	0.48	2.32	2.49	0.68	2.28	2.11	0.85	2.71	2.29
	Median	221.48	42.15	179.66	221.48	25.10	196.50	221.48	17.14	25.10
	Range	2.58	12.10	13.69	4.44	10.36	7.52	6.40	15.54	10.62
	Number	35	35	36	34	34	36	36	36	36
4	Average	221.05	45.71	175.37	221.04	27.79	193.19	221.10	17.82	27.91
	Std. Dev.	2.18	2.76	4.21	2.40	2.59	2.52	2.42	3.44	2.62
	Median	221.48	45.23	176.22	221.48	28.88	192.91	221.48	17.05	28.88
	Range	13.99	13.13	26.08	15.49	9.83	11.81	17.69	15.91	10.45
	Number	36	36	37	35	35	37	37	37	37
5	Average	458.85	90.16	368.74	458.86	52.91	406.05	458.90	37.31	52.85
	Std. Dev.	1.05	7.66	8.22	1.62	6.71	6.68	2.08	7.12	6.94
	Median	459.25	91.09	368.63	459.25	54.32	405.43	459.25	35.92	54.08
	Range	4.76	33.42	37.27	10.74	32.54	28.57	15.12	40.65	32.76
	Number	33	35	34	32	34	34	34	34	34
6	Average	458.96	98.06	361.09	459.08	61.54	397.70	459.14	36.63	61.43
	Std. Dev.	0.84	8.63	8.87	1.15	6.94	7.30	1.88	5.30	7.22
	Median	459.25	97.40	362.73	459.26	63.41	397.12	459.25	36.15	63.41
	Range	4.02	29.77	29.74	7.32	30.17	30.44	12.25	20.90	30.17
	Number	32	34	33	31	33	33	33	33	33

TABLE 10. (Continued)

Case	Statistic	Surface			Tropopause			Top		
		Up	Down	Net	Up	Down	Net	Up	Dnet1	Dnet2
7	Average	458.72	80.87	377.78	407.22	7.10	400.21	411.98	22.66	11.56
	Std. Dev.	1.05	4.51	4.92	4.52	1.18	5.31	7.47	4.40	6.95
	Median	459.25	81.89	377.07	408.57	6.82	401.72	411.91	23.51	10.21
	Range	4.02	20.47	22.65	23.56	6.04	28.04	52.95	15.53	43.74
8	Number	36	36	37	33	33	36	37	36	36
	Average	458.80	88.25	370.46	401.33	8.40	393.06	406.39	22.85	13.05
	Std. Dev.	0.98	4.87	5.12	4.38	1.34	5.21	3.86	5.25	2.34
	Median	459.25	89.58	369.62	402.24	8.14	394.52	407.33	23.84	12.79
9	Range	4.02	19.43	19.47	20.67	6.54	25.34	19.26	20.06	11.88
	Number	35	35	36	32	32	35	36	35	35
	Average	423.21	75.77	347.41	381.99	13.17	368.85	382.66	21.66	13.61
	Std. Dev.	0.91	4.18	4.48	3.20	1.83	4.64	3.35	3.83	2.20
10	Median	423.60	76.65	346.22	383.24	12.62	370.13	383.32	22.40	13.18
	Range	3.48	20.20	21.84	17.64	9.96	25.76	18.82	16.03	12.25
	Number	37	37	38	35	35	37	38	37	37
	Average	423.27	82.58	340.66	377.29	15.13	362.21	378.87	21.79	16.44
11	Std. Dev.	0.83	4.34	4.53	3.07	1.87	4.46	3.30	4.41	2.88
	Median	423.60	83.60	340.02	377.81	14.49	363.32	379.21	22.17	15.80
	Range	3.23	17.98	17.94	15.17	9.78	23.15	15.19	19.11	14.12
	Number	36	36	37	34	34	36	37	36	36
12	Average	311.07	56.05	255.03	285.85	15.81	270.09	283.52	15.22	13.32
	Std. Dev.	0.62	3.40	3.62	2.24	2.20	4.04	2.38	2.32	2.00
	Median	311.26	56.00	255.42	286.75	15.19	271.64	284.19	15.00	12.98
	Range	3.19	17.80	18.21	11.93	12.59	21.64	12.00	10.54	12.81
13	Number	35	35	36	33	33	35	36	35	35
	Average	311.13	60.86	250.27	283.01	17.72	265.34	280.87	15.24	15.42
	Std. Dev.	0.52	3.01	3.11	2.16	2.26	3.84	2.19	2.71	2.15
	Median	311.26	60.90	250.36	283.55	17.21	266.48	281.41	15.04	15.14
14	Range	3.07	13.75	14.16	10.41	12.03	19.80	9.55	12.75	13.67
	Number	34	34	35	32	32	34	35	34	34
	Average	384.36	68.25	316.09	350.85	18.35	332.58	350.12	16.69	17.38
	Std. Dev.	0.78	3.83	4.11	2.74	2.20	4.56	2.75	2.86	2.58
15	Median	384.68	68.59	316.04	351.72	17.80	334.01	350.70	16.90	17.09
	Range	3.41	19.47	20.59	14.18	12.03	25.09	14.60	11.50	15.16
	Number	35	35	36	33	33	35	36	35	35
	Average	384.42	74.39	310.01	347.24	20.69	326.64	346.97	16.85	20.15
16	Std. Dev.	0.70	3.76	3.91	2.61	2.13	4.27	2.55	3.44	2.65
	Median	384.68	74.89	309.30	347.81	20.11	327.70	347.57	16.80	19.70
	Range	3.22	14.95	15.78	12.18	10.78	22.36	12.09	15.31	16.02
	Number	34	34	35	32	32	34	35	34	34
17	Average	247.63	45.75	201.92	230.93	15.62	215.29	229.14	13.52	13.78
	Std. Dev.	0.50	3.06	3.22	1.74	2.04	3.53	1.91	2.45	1.96
	Median	247.73	45.42	202.75	231.42	15.08	216.68	229.78	13.03	13.50
	Range	2.90	15.95	15.95	9.41	11.12	19.40	10.47	15.52	12.71
18	Number	36	36	37	33	33	36	37	36	36
	Average	247.68	49.49	198.21	228.97	17.58	211.37	227.18	13.31	15.73
	Std. Dev.	0.42	2.62	2.66	1.67	1.98	3.37	1.69	2.11	2.01
	Median	247.73	49.51	198.30	229.44	16.97	212.70	227.92	13.32	15.39
19	Range	2.82	12.48	12.47	8.35	10.01	17.52	7.20	10.83	12.75
	Number	35	35	36	32	32	35	36	35	35
	Average	423.18	305.14	118.15	329.65	5.93	323.82	329.78	206.12	5.91
	Std. Dev.	0.91	13.29	12.84	6.61	1.18	5.90	6.00	14.62	1.61
20	Median	423.60	306.09	117.90	331.35	5.92	325.34	331.24	210.14	5.80
	Range	3.48	53.31	53.19	32.90	6.96	29.00	32.36	67.99	10.08
	Number	33	33	34	30	30	32	34	32	32
	Average	423.27	263.20	160.05	334.74	5.74	328.96	334.53	168.56	5.54
18	Std. Dev.	0.81	14.77	14.37	7.77	1.42	6.82	7.45	11.46	1.47
	Median	423.60	259.50	162.67	337.16	5.90	330.59	336.60	168.36	5.80
	Range	3.23	64.33	63.83	37.51	7.14	35.03	37.51	61.87	7.57
	Number	33	33	34	31	31	33	34	33	33
19	Average	422.97	326.23	96.71	322.09	6.93	315.31	322.05	219.19	6.65
	Std. Dev.	1.40	14.06	13.42	7.67	1.39	7.29	7.25	15.52	1.42
	Median	423.58	329.30	94.33	323.90	6.80	317.29	323.75	225.88	6.63
	Range	7.50	57.55	57.28	37.65	7.62	37.50	37.56	66.86	8.20
20	Number	36	36	37	33	33	35	37	35	35
	Average	423.24	273.19	150.22	329.06	6.63	322.45	328.79	171.80	6.33
	Std. Dev.	0.86	17.82	17.41	9.78	1.50	8.93	9.38	12.24	1.59
	Median	423.60	268.40	153.96	332.48	6.80	324.70	331.10	171.49	6.65
20	Range	3.23	74.93	74.43	47.14	7.93	47.03	46.86	61.59	8.31
	Number	35	35	36	33	33	35	36	35	35

TABLE 10. (Continued)

Case	Statistic	Surface			Tropopause			Top		
		Up	Down	Net	Up	Down	Net	Up	Dnet1	Dnet2
21	Average	423.19	344.19	78.79	316.99	7.63	309.48	316.86	231.54	7.31
	Std. Dev.	0.91	15.88	15.50	5.39	1.43	4.88	5.09	15.55	1.42
	Median	423.60	349.70	74.60	317.85	7.63	310.80	318.10	237.33	7.36
	Range	3.48	67.22	66.95	26.60	8.24	20.50	26.38	62.31	8.43
	Number	33	33	34	30	30	32	34	32	32
22	Average	423.27	279.76	143.56	325.86	7.41	318.43	325.55	174.33	7.15
	Std. Dev.	0.82	16.70	16.27	7.47	1.69	6.42	7.21	12.89	1.75
	Median	423.60	275.20	147.29	328.89	7.63	320.25	327.00	173.60	7.42
	Range	3.23	71.80	71.30	31.86	8.55	29.51	32.21	61.96	8.96
	Number	33	33	34	31	31	33	34	33	33
23(a)	Average	423.25	1.42	421.82	422.96	0.98	421.90	421.05	0.18	-0.84
	Std.Dev.	0.79	0.36	0.84	0.82	0.36	0.88	0.84	0.11	0.18
	Median	423.44	1.58	422.07	423.30	1.14	422.23	421.31	0.17	-0.86
	Range	3.12	1.42	3.34	3.03	1.27	2.90	3.17	0.37	0.64
	Number	12	12	12	11	12	11	11	11	11
23(b)	Average	423.21	5.69	417.52	419.30	2.29	416.97	413.26	-0.43	-3.65
	Std.Dev.	0.88	3.26	3.25	1.62	0.74	2.02	2.10	1.90	1.82
	Median	423.60	4.84	418.73	420.06	2.20	417.85	413.70	-0.86	-3.99
	Range	3.48	16.50	16.44	7.47	4.17	9.94	12.80	10.97	9.96
	Number	32	32	33	28	29	30	32	30	30
23(c)	Average	421.46	6.33	415.13	417.54	2.74	414.80	410.64	-0.32	-4.17
	Std.Dev.	6.47	1.71	7.99	7.07	0.97	6.67	6.10	1.49	1.24
	Median	423.54	6.30	417.32	419.59	3.21	416.59	411.70	-0.73	-4.48
	Range	26.76	7.93	33.92	29.83	3.20	30.05	29.67	6.01	4.15
	Number	15	15	15	15	15	15	15	15	15
24(a)	Average	423.50	5.70	417.80	419.18	2.11	417.07	414.04	-0.58	-3.05
	Std.Dev.	0.43	3.17	3.06	1.71	0.84	2.42	0.72	0.78	2.05
	Median	423.60	4.74	418.92	420.04	1.98	418.07	414.34	-0.81	-3.73
	Range	1.80	11.41	11.08	5.87	3.38	8.32	2.36	2.72	7.86
	Number	11	11	11	10	10	10	11	10	10
24(b)	Average	423.23	5.83	417.40	419.17	2.60	416.57	412.71	-0.83	-3.86
	Std.Dev.	0.83	0.79	1.13	1.00	0.48	1.16	1.01	0.31	0.56
	Median	423.60	6.17	417.74	419.77	2.76	417.05	412.61	-0.75	-3.75
	Range	2.83	3.14	3.97	2.96	1.66	4.12	4.15	1.20	2.05
	Number	9	9	9	9	9	9	9	9	9
24(c)	Average	423.50	6.40	417.10	418.06	2.41	378.35	375.53	-0.69	-2.82
	Std.Dev.	0.43	3.23	3.12	2.18	0.85	119.67	118.75	0.84	2.26
	Median	423.60	5.44	418.25	419.38	2.23	417.21	413.31	-0.99	-3.51
	Range	1.80	11.69	11.36	6.23	3.49	417.44	413.85	2.97	8.26
	Number	11	11	11	11	11	11	11	11	11
24(d)	Average	423.23	6.81	416.42	418.68	3.11	415.57	411.26	-0.85	-4.31
	Std.Dev.	0.83	0.95	1.22	0.88	0.61	1.26	1.32	0.23	0.74
	Median	423.60	7.26	416.77	419.05	3.48	416.03	411.22	-0.84	-4.29
	Range	2.83	3.64	4.19	2.57	2.12	4.37	5.41	0.63	2.61
	Number	9	9	9	9	9	9	9	9	9
25	Average	458.63	390.99	67.35	293.64	11.94	282.03	292.17	214.89	10.17
	Std. Dev.	1.29	11.51	11.29	7.26	3.22	8.12	6.93	12.49	4.00
	Median	459.21	392.25	66.49	294.64	11.42	283.57	293.93	220.06	9.66
	Range	6.27	55.12	55.61	33.94	20.11	33.05	31.53	59.32	26.53
	Number	38	38	40	34	34	38	40	38	38
26	Average	458.81	392.24	66.50	289.25	12.76	276.69	289.16	210.66	12.33
	Std. Dev.	0.99	11.54	11.39	7.65	1.90	7.81	7.29	12.49	2.48
	Median	459.25	393.44	65.81	290.58	12.44	278.22	290.81	217.11	12.36
	Range	4.02	54.39	54.88	35.17	9.83	31.54	32.70	57.46	13.89
	Number	33	33	34	30	30	33	34	33	33
27	Average	423.07	343.18	79.86	289.20	22.44	267.02	283.90	187.13	16.94
	Std. Dev.	1.15	8.21	7.86	6.42	3.17	7.25	6.00	9.98	3.71
	Median	423.59	343.36	80.25	291.21	22.08	269.02	285.74	190.21	16.40
	Range	5.83	41.86	42.23	29.46	16.32	31.77	26.32	43.34	26.34
	Number	39	39	41	35	35	39	41	39	39
28	Average	423.10	344.73	78.46	285.52	24.38	261.31	281.09	182.98	19.70
	Std. Dev.	1.15	8.40	8.19	6.75	3.34	7.81	6.36	10.18	4.12
	Median	423.60	344.13	78.82	286.03	23.63	263.46	282.82	187.00	18.99
	Range	5.67	41.43	41.80	30.07	16.85	33.51	27.99	42.20	27.19
	Number	34	34	35	32	32	34	35	34	34
29	Average	310.95	215.88	95.16	240.51	30.91	209.79	231.99	114.51	22.25
	Std. Dev.	0.95	6.14	6.00	4.60	4.35	6.31	4.46	7.17	3.41
	Median	311.26	215.50	95.80	241.60	31.30	211.71	233.89	115.65	22.28
	Range	5.75	34.00	33.96	19.05	19.75	24.38	16.43	31.92	18.85
	Number	37	37	39	34	34	37	39	37	37

TABLE 10. (Continued)

TABLE 10. (Continued)

Case	Statistic	Surface			Tropopause			Top:		
		Up	Down	Net	Up	Down	Net	Up	Dnet1	Dnet2
42	Average	458.82	411.78	47.05	458.82	236.08	224.88	458.82	177.83	233.94
	Std. Dev.	0.81	12.36	12.42	0.81	20.42	19.78	0.80	17.76	19.83
	Median	459.25	414.35	46.76	459.25	234.90	224.52	459.25	179.89	234.73
	Range	2.88	54.30	54.37	2.88	62.09	60.82	2.87	67.44	62.09
	Number	14	14	14	14	14	14	14	14	14
43	Average	458.88	327.58	131.08	458.88	211.34	247.47	458.88	116.39	211.41
	Std. Dev.	0.80	20.44	20.38	0.80	22.48	22.53	0.79	25.71	22.43
	Median	459.25	323.85	137.45	459.25	212.22	249.37	459.25	116.17	212.22
	Range	3.23	69.48	69.55	3.23	87.34	87.78	3.23	114.78	87.34
	Number	15	15	15	15	15	15	15	15	15
44	Average	423.44	169.84	253.60	405.43	0.00	405.43	405.42	151.83	0.00
	Std. Dev.	0.40	74.28	74.34	9.64	0.01	9.64	9.64	64.91	0.00
	Median	423.60	193.20	240.07	406.20	0.00	406.20	406.20	171.70	0.00
	Range	1.47	287.81	287.83	37.23	0.04	37.23	37.23	250.61	0.01
	Number	12	12	12	12	12	12	12	12	12
45	Average	423.41	83.48	339.98	409.69	0.07	409.62	409.65	69.64	0.03
	Std. Dev.	0.45	59.75	59.74	16.25	0.12	16.35	16.28	45.21	0.08
	Median	423.60	98.22	336.93	415.28	0.00	415.28	415.28	81.66	0.00
	Range	1.47	209.82	209.82	54.99	0.35	55.34	55.11	154.49	0.26
	Number	9	9	9	9	9	9	9	9	9
46	Average	458.97	218.60	240.38	427.26	0.00	427.26	427.26	186.89	0.00
	Std. Dev.	0.52	84.51	84.56	15.58	0.01	15.58	15.58	69.56	0.01
	Median	459.25	243.10	226.14	427.68	0.00	427.68	427.68	206.10	0.00
	Range	1.62	335.00	335.02	63.60	0.03	63.60	63.60	271.42	0.03
	Number	12	12	12	12	12	12	12	12	12
47	Average	458.91	102.28	356.63	439.82	0.02	439.81	439.80	83.17	0.00
	Std. Dev.	0.63	67.85	67.70	20.95	0.02	20.97	20.96	49.66	0.01
	Median	459.25	120.34	348.28	446.21	0.00	446.21	446.21	98.10	0.00
	Range	1.62	237.65	237.66	72.99	0.06	73.04	73.03	164.62	0.05
	Number	9	9	9	9	9	9	9	9	9
48	Average	221.42	41.17	180.25	221.42	24.35	197.07	221.42	16.82	24.35
	Std. Dev.	0.21	2.21	2.30	0.21	2.30	2.40	0.21	1.53	2.30
	Median	221.48	41.83	180.17	221.48	25.10	197.22	221.48	16.73	25.10
	Range	0.89	7.44	7.60	0.89	8.23	8.39	0.89	4.59	8.23
	Number	12	12	12	12	12	12	12	12	12
49	Average	221.42	45.00	176.42	221.42	27.98	193.45	221.42	17.03	27.98
	Std. Dev.	0.21	2.33	2.41	0.21	2.45	2.56	0.21	1.67	2.45
	Median	221.48	45.22	176.51	221.48	27.92	193.64	221.48	16.97	27.92
	Range	0.89	7.37	7.55	0.89	8.58	8.76	0.89	6.00	8.58
	Number	12	12	12	12	12	12	12	12	12
50	Average	459.02	80.86	378.16	459.02	48.43	410.59	459.02	32.43	48.43
	Std. Dev.	0.50	4.28	4.58	0.50	5.31	5.54	0.50	3.33	5.31
	Median	459.25	81.52	378.47	459.25	49.24	410.40	459.25	32.03	49.24
	Range	1.99	14.80	16.13	1.99	23.41	23.68	1.99	11.78	23.41
	Number	12	12	12	12	12	12	12	12	12
51	Average	459.02	88.75	370.27	459.02	55.57	403.45	459.02	33.19	55.57
	Std. Dev.	0.50	4.78	5.03	0.50	5.60	5.85	0.50	4.13	5.60
	Median	459.25	89.81	369.85	459.25	56.32	404.40	459.25	34.15	56.32
	Range	1.99	15.16	16.50	1.99	24.25	24.52	1.99	14.72	24.25
	Number	12	12	12	12	12	12	12	12	12
52	Average	423.14	327.00	96.13	297.61	21.24	276.36	293.01	181.43	16.60
	Std. Dev.	0.89	4.54	4.65	5.59	1.78	5.82	5.94	4.46	3.10
	Median	423.60	326.91	96.95	299.75	21.25	279.27	294.54	183.35	15.47
	Range	2.89	17.69	17.71	21.74	6.00	17.47	25.90	17.28	11.05
	Number	15	15	15	15	15	15	15	15	15
53	Average	423.35	296.64	126.71	301.17	20.96	280.22	296.00	153.51	15.78
	Std. Dev.	0.65	6.73	6.81	5.87	1.80	6.06	5.04	4.19	2.56
	Median	423.60	297.14	126.79	303.14	21.22	282.21	296.53	154.45	15.15
	Range	2.57	26.10	25.76	20.12	6.00	18.76	19.68	15.50	10.51
	Number	14	14	14	14	14	14	14	14	14
54	Average	423.14	359.98	63.15	286.71	22.96	263.76	282.30	200.60	18.54
	Std. Dev.	0.89	7.08	6.74	5.53	1.96	5.91	5.73	7.22	3.10
	Median	423.60	362.36	64.13	289.19	23.04	266.92	284.12	203.70	17.47
	Range	2.89	27.32	27.30	20.17	6.54	18.19	23.56	29.02	10.73
	Number	15	15	15	15	15	15	15	15	15
55	Average	423.35	307.01	116.34	293.77	22.61	271.17	288.66	154.84	17.49
	Std. Dev.	0.65	8.07	8.07	6.42	1.99	6.57	5.52	5.36	2.70
	Median	423.60	306.53	117.47	296.04	22.79	273.81	289.72	155.46	16.94
	Range	2.57	34.24	33.89	21.61	6.54	19.63	21.27	23.01	11.18
	Number	14	14	14	14	14	14	14	14	14

The terms up, down, and net refer to the upward, downward, and net upward flux components, respectively; Dnet1 and Dnet2 are the differences between the net fluxes at the tropopause and surface and at the top of the atmosphere and tropopause, respectively; and number is the number of model calculations. All fluxes are in W m⁻².

TABLE 11. Same as Table 10 but for the Cloudy-Sky Study

Case	Statistic	Surface			Tropopause			Top		
		Up	Down	Net	Up	Down	Net	Up	Dnet1	Dnet2
1	Average	423.33	360.43	62.87	163.65	22.47	141.18	165.06	78.31	23.88
	Std. Dev.	0.77	6.74	6.71	21.01	1.71	22.11	18.75	17.24	3.89
	Median	423.60	357.52	66.08	164.77	22.21	140.50	164.40	82.61	24.85
	Range	2.89	23.10	23.30	77.42	6.51	80.91	66.28	63.04	14.63
	Number	12	12	12	12	12	12	12	12	12
2	Average	423.34	398.97	24.37	280.57	22.50	257.16	276.05	232.79	18.89
	Std. Dev.	0.81	8.02	7.91	7.88	1.78	7.17	8.38	7.80	5.32
	Median	423.60	398.08	26.73	282.46	22.61	259.85	277.07	234.31	17.22
	Range	2.89	28.08	28.09	30.59	6.51	24.86	33.68	30.43	21.46
	Number	11	11	11	11	11	11	11	11	11
3	Average	423.56	358.29	65.28	194.17	22.30	171.87	193.91	106.60	22.03
	Std. Dev.	0.00	6.78	6.82	23.02	2.23	21.90	22.23	24.71	1.30
	Median	423.60	363.78	66.42	201.29	23.42	179.10	201.95	119.50	22.85
	Range	0.24	20.10	20.17	61.19	7.31	60.98	59.23	75.84	4.28
	Number	7	7	7	7	7	7	7	7	7
4	Average	423.49	361.10	62.39	125.42	21.89	103.53	129.82	41.14	26.29
	Std. Dev.	0.38	7.22	7.27	6.35	2.20	7.20	5.26	7.32	3.83
	Median	423.61	362.00	62.50	124.63	22.19	104.18	129.00	42.08	26.73
	Range	1.80	24.22	24.43	27.62	7.31	27.72	21.98	29.19	15.46
	Number	13	13	13	13	13	13	13	13	13
5	Average	423.56	388.74	34.81	283.80	22.29	261.51	279.83	226.70	18.33
	Std. Dev.	0.00	11.09	11.10	7.55	2.08	9.13	10.15	15.13	1.84
	Median	423.60	390.69	34.53	283.02	22.21	262.02	278.11	233.23	17.96
	Range	0.19	34.79	34.95	25.59	7.31	30.19	33.71	49.56	5.99
	Number	8	8	8	8	8	8	8	8	8
6	Average	423.52	412.69	10.83	276.98	21.99	254.99	273.47	244.16	18.48
	Std. Dev.	0.31	2.54	2.42	7.15	2.06	8.26	8.68	7.71	2.48
	Median	423.60	414.24	10.01	276.98	22.21	254.37	272.72	245.36	18.15
	Range	1.80	7.91	7.93	32.22	7.31	36.51	39.67	30.63	10.91
	Number	15	15	15	15	15	15	15	15	15

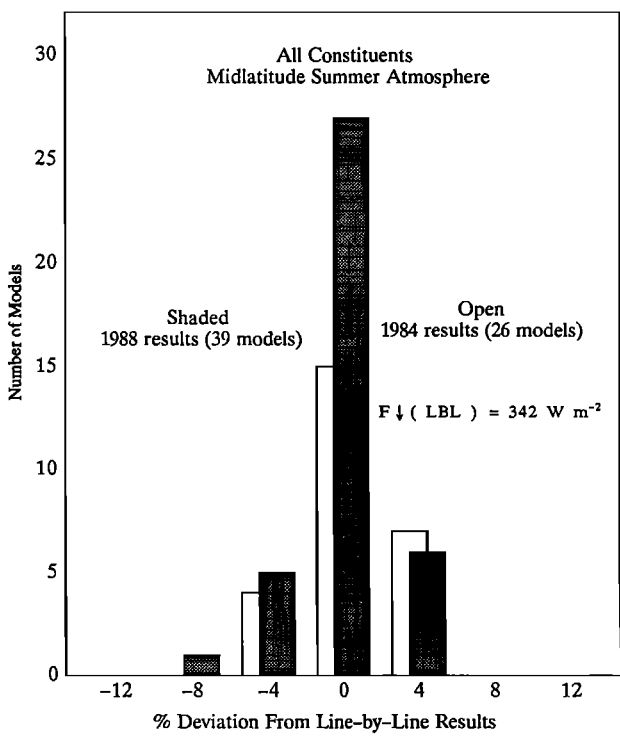


Fig. 4. A comparison of the 1984 (open) and 1988 (shaded) distributions of downward fluxes at the surface relative to the Fels-Schwarzkopf (GFDL) line-by-line calculations (LBL) for the AFGL mid-latitude summer profile when H₂O, O₃, and 300 ppmv CO₂ are included in the calculations. Note that the width of each histogram bar is 4% of the LBL calculation, the 1988 distribution is offset slightly for better viewing, and the distributions include LBL model results, one for 1984 and three for 1988.

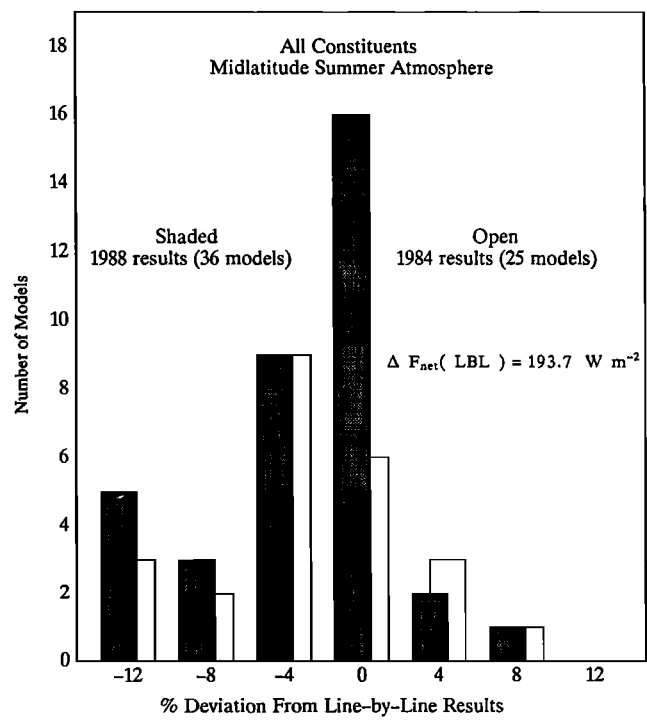


Fig. 5. As in Figure 1 but for the flux divergence of the troposphere (0–13 km). Note that the 1984 distribution is offset slightly for better viewing.

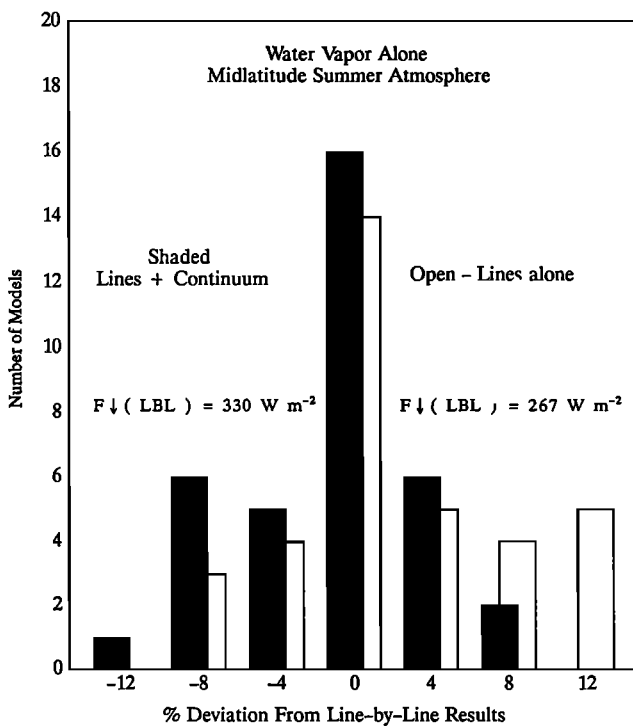


Fig. 6. The 1988 distributions of the flux differences relative to the GFDL line-by-line results when the water vapor lines only (open) and the lines plus the continuum (shaded) are included in the calculations. Note that the lines only distribution is offset slightly for better viewing.

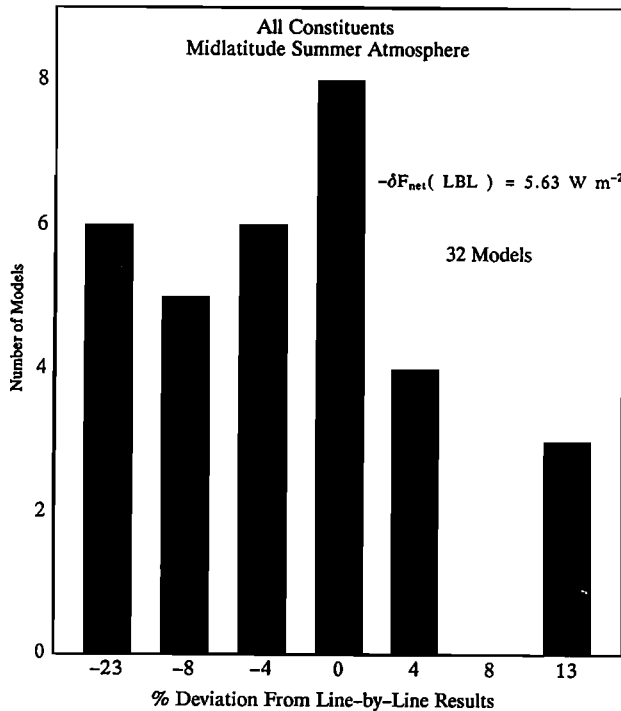


Fig. 7. The distribution of the change in the net flux at the tropopause as CO₂ doubles from 300 ppmv relative to the GFDL line-by-line calculations for mid-latitude summer conditions with all constituents. Note that the histogram bar at the positive (negative) end of the distribution is labeled with the average value of data greater (less) than the limit of the previous interval.

TABLE 12. Categories of Narrow- and Wide-Band Models

Category	Explanation
Narrow-Band Model Categories	
1	Line-by-line models
2	Analytic band model with $\Delta\nu = 5 \text{ cm}^{-1}$
3	Analytic band models with $5 < \Delta\nu < 50 \text{ cm}^{-1}$
4	Analytic band models with $\Delta\nu > 50 \text{ cm}^{-1}$
5	k -distribution models fit to band model results
6	k -distribution models fit to line-by-line results
Broad-Band Model Categories	
1	Line-by-line models
2	Parameterized line-by-line results
3	Broadband model fit to spectral data
4	Band model fit to NBM results over several wide intervals
5	Laboratory emissivity data
6	Other (details not specific)

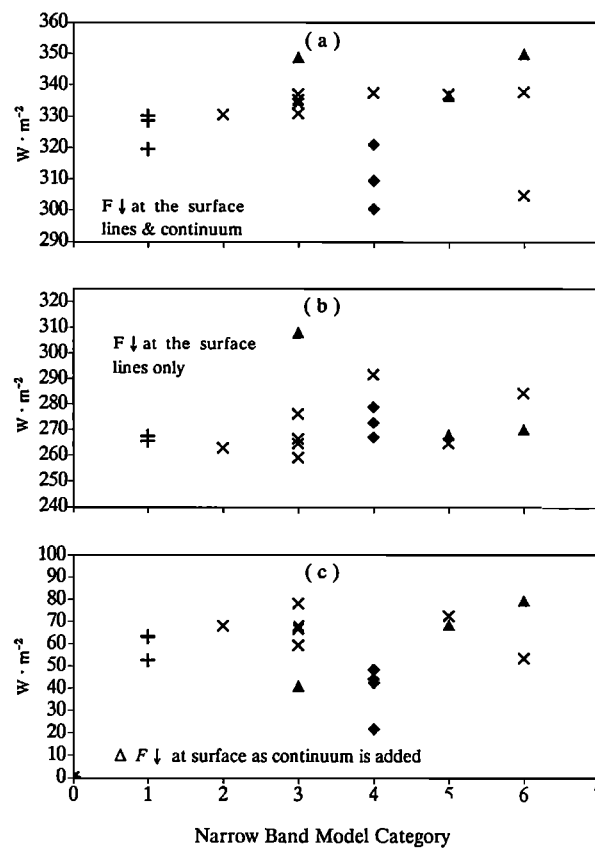


Fig. 8. Narrow-band model calculations of $F \downarrow$ at the surface when water vapor is the only active gas: (a) lines and the continuum, (b) lines alone, and (c) a minus b . The temperature distribution of the mid-latitude summer atmosphere is used in the calculations. Model categories are explained in Table 12.

Thus the sources of continuum and spectral line data do not, in general, appear to be a major cause of discrepancy between model results.

The search for other explanations has led to the discovery, shown in Figure 15, that the outliers to the model calculations are largely associated with participants who have not tested the

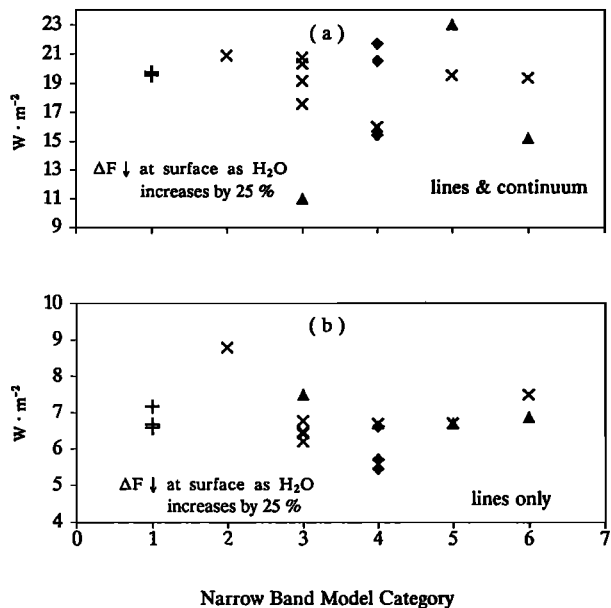


Fig. 9. Narrow-band model calculations of the change in $F \downarrow$ at the surface as the H_2O concentration at all levels of the mid-latitude summer atmosphere conditions increases by 25%: (a) lines and continuum, and (b) lines alone.

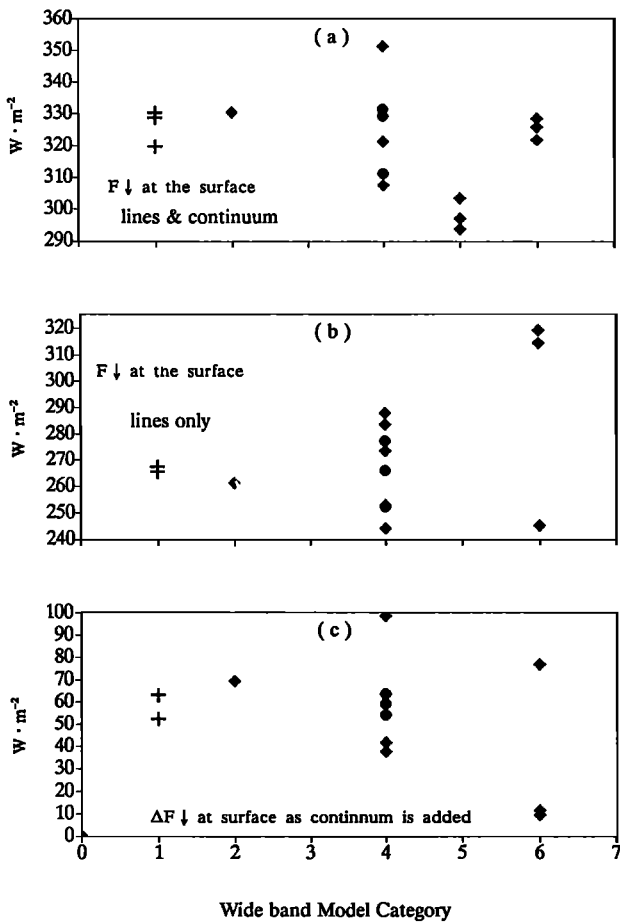


Fig. 10. As in Figure 8 but for the wide-band models.

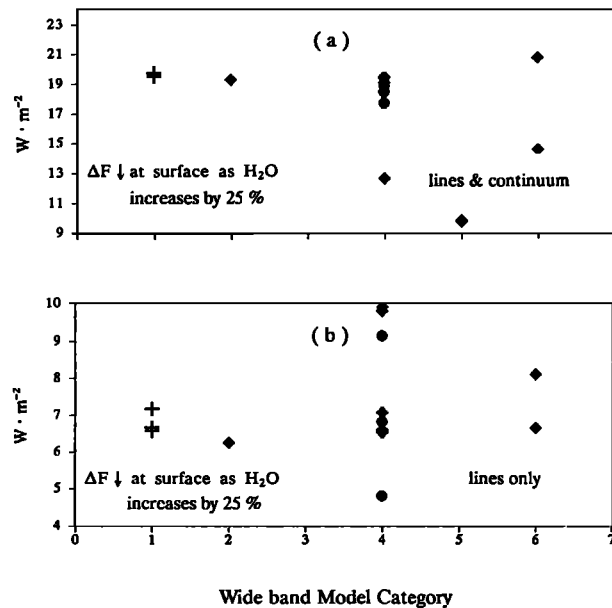


Fig. 11. As in Figure 9 but for the wide-band models.

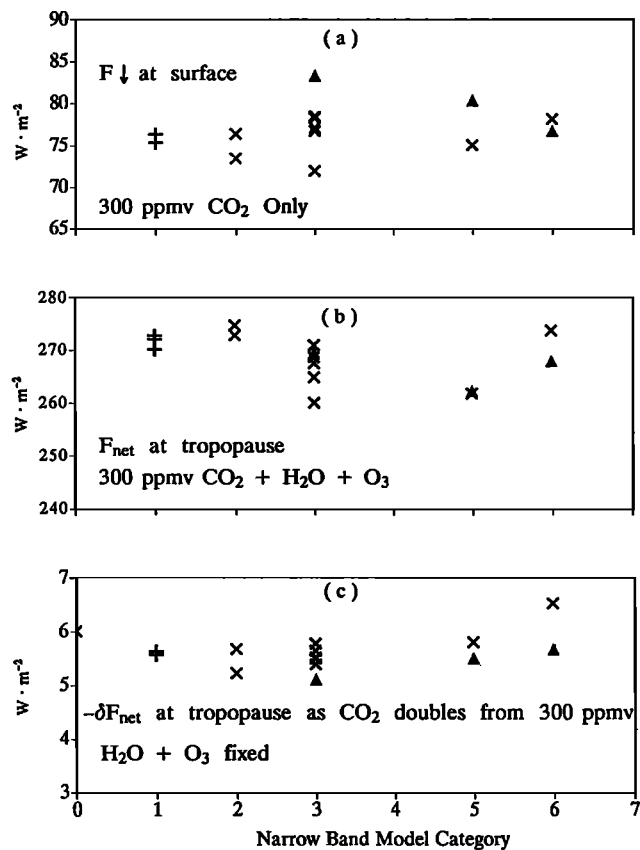


Fig. 12. Narrow-band model calculations of (a) $F \downarrow$ at the surface when CO_2 is the only active gas; (b) F_{net} at the tropopause with $300 \text{ ppmv } CO_2, H_2O$ and O_3 ; and (c) $-\delta F_{net}$ as CO_2 doubles from 300 ppmv while keeping H_2O and O_3 fixed. All calculations use the mid-latitude summer profile, and the model categories are defined in Table 12.

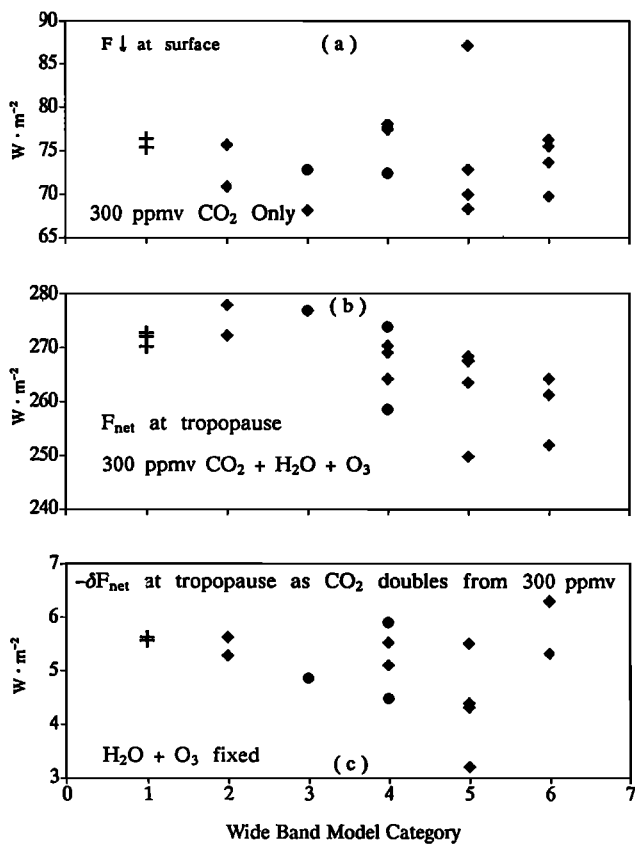


Fig. 13. As in Figure 12 but for the wide-band models.

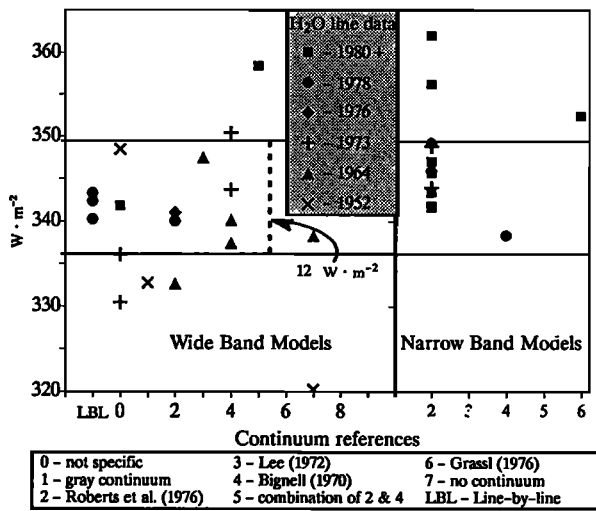


Fig. 14. Model calculations of $F \downarrow$ at the surface as a function of the reference for the H_2O continuum and the date of the H_2O spectral line data. All calculations use 300 ppmv CO_2 , and the H_2O , O_3 , and temperature distributions of the mid-latitude summer profile.

accuracy of their technique used to perform the integration over altitude (hereafter denoted as z -tested). For the MLS atmosphere, all z -tested models yield values of $F \downarrow$ at the surface within 12 W m^{-2} of each other and within about $\pm 2\%$ of the LBL calculations. For F_{net} at the tropopause, seven of the nine

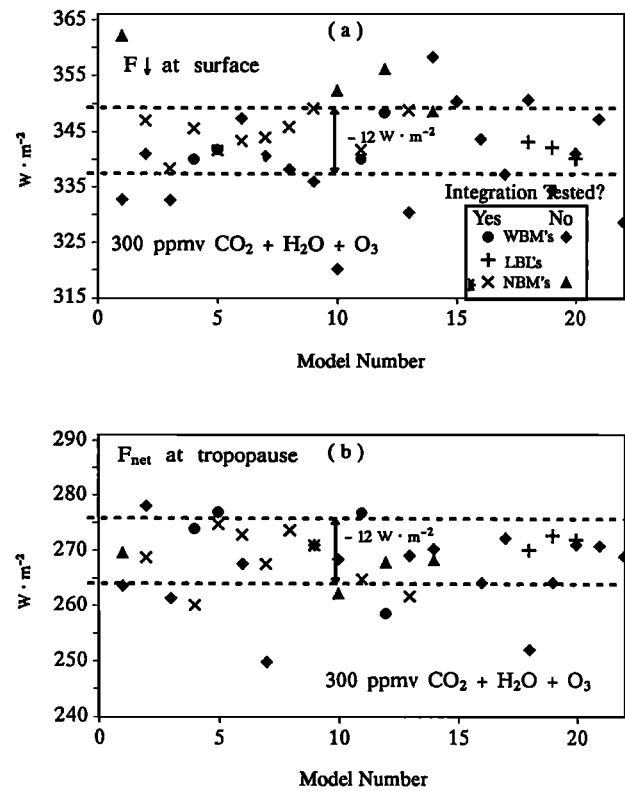


Fig. 15. Distributions of model calculations of (a) $F \downarrow$ at the surface and (b) F_{net} at the tropopause using 300 ppmv CO_2 , and the H_2O , O_3 , and temperature distributions of the mid-latitude summer atmosphere. The symbols given in the box of (a) denote whether or not the vertical integration of a model has been tested for accuracy by its developer.

z -tested NBMs fall within the 12 W m^{-2} range, as do three of the four z -tested WBMs. Similar good agreement is found for the net flux divergence for the troposphere (ΔF_{net}) (Figure 16a) between most of the z -tested models.

Overall, the majority of z -tested calculations of $F \downarrow$ and F_{net} tend to agree with each other to within about 12 W m^{-2} for each of the model atmospheres (Figures 17 and 18). Note, however, that requiring numerical accuracy in the altitude integration for $F \downarrow$ at the surface does not insure accuracy for ΔF_{net} for the troposphere, or vice versa. In general, the spread between the model calculations decreases as the atmosphere becomes colder and drier. This indicates that part of the outlier problem may be related to differences in the parameterization of the H_2O continuum and its temperature dependence. However, it is difficult to search for these effects in models lacking accurate altitude integrations.

Most of the variation in the CO_2 doubling case (Figure 16b) comes from the wide band models. Six of 17 WBMs and 11 of 13 NBM results come within $\pm 5\%$ of the line-by-line results. However, only two of the four z -tested WBMs fall within this range as compared with eight of nine z -tested NBMs. Of the WBMs that agreed well with the LBL results about which we had information, four were developed using LBL model results, one was fit to laboratory observations, and the others used an analytic band model fit to spectral line data (only four of the six appear to different parameterizations, however). Since the LBL calculations for CO_2 appear to be adequately tested with laboratory

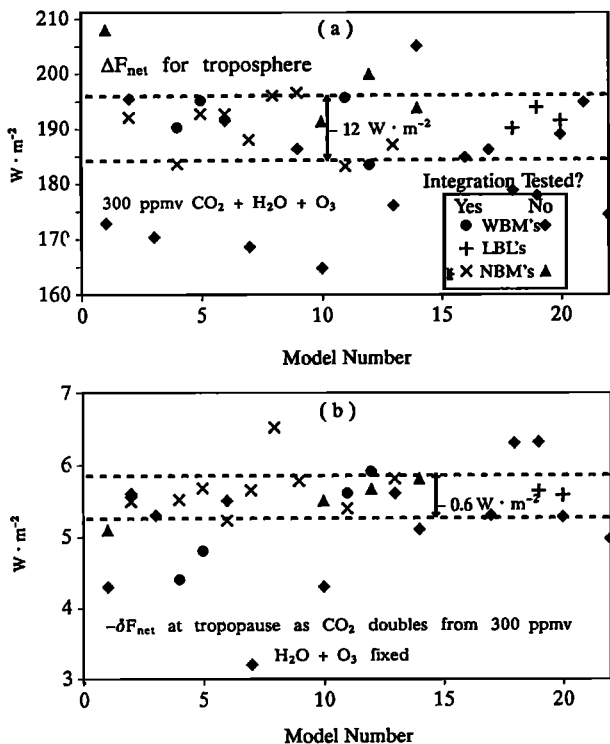


Fig. 16. Distributions of model calculations of (a) the net flux difference for the troposphere (ΔF_{net}) and (b) the change in the net flux at the tropopause ($-\delta F_{\text{net}}$) as CO₂ doubles from 300 ppmv. Symbols are as in Figure 15.

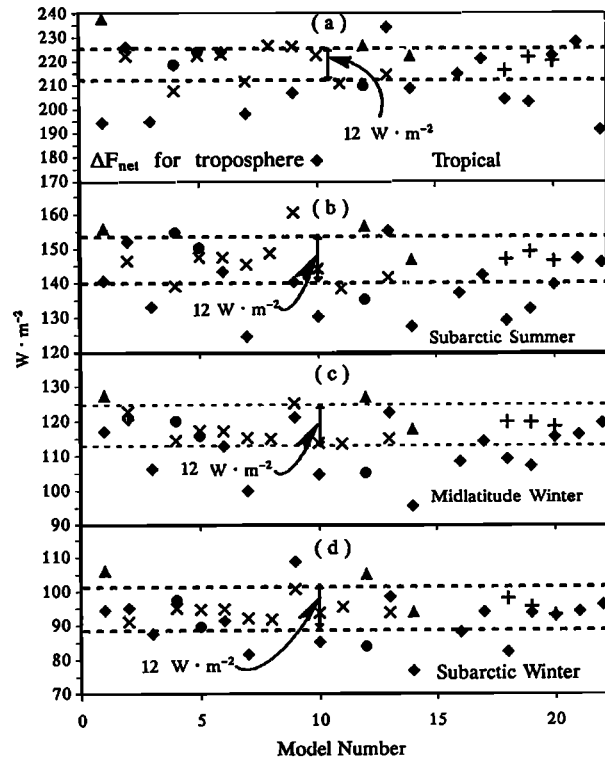


Fig. 18. As in Figure 17 but for ΔF_{net} .

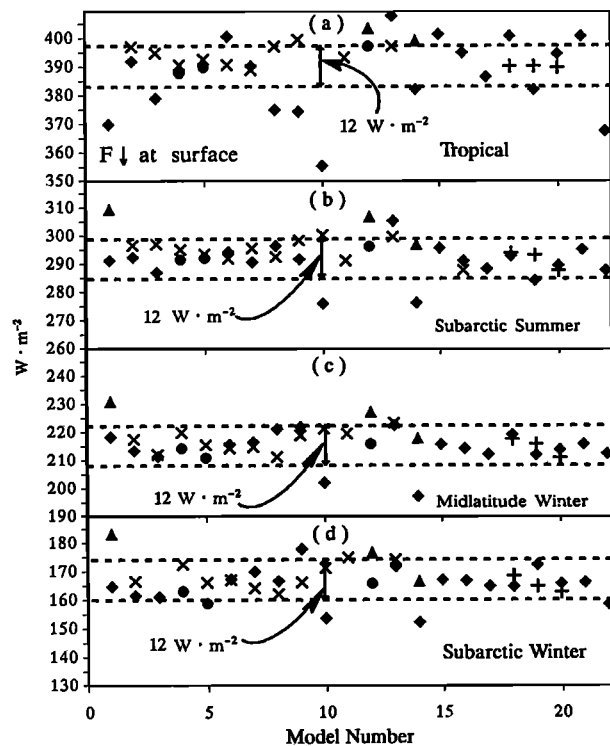


Fig. 17. Distributions of model calculations of F_{\downarrow} at the surface using 300 ppmv CO₂, and the H₂O, O₃, and temperature distributions of the (a) tropical, (b) subarctic summer, (c) midlatitude winter, and (d) subarctic winter atmospheres. Symbols are as in Figure 15.

data, we attribute the z -tested outliers to inadequate modeling of CO₂ absorption.

Good agreement between the WBM and LBL results for the doubled CO₂ case has little association with good agreement for F_{\downarrow} and ΔF_{net} . Of the seven WBMs that agreed well with the LBL F_{\downarrow} and ΔF_{net} results, only four did well on the doubled CO₂ test. Conversely, two models that were within 10% of the LBL results for the doubled CO₂ tests had very poor agreement in the flux comparisons.

Having ascertained those models that have not been z -tested, the reader may wish to review the calculations presented as functions of model categories which have been codified according to Figure 15.

Detracting from the convenient way of evaluating the models is the finding that only four of the wide-band modelers claimed to have actually tested their technique for performing the altitude integration. In fairness, a few of the modelers checked neither yes or no to having tested their models, and those models for which we had no questionnaires were grouped there as well. We suspect that such tests were done with a few of the models at some stage in their development because a few "untested" models give extraordinarily good comparisons with the line-by-line results. The lack of testing of some of the models may in part be due to the radiation codes being used in climate models having coarse resolution. However, this is not a valid excuse for improving the calculations by adding extra resolution for use only in the radiation code.

4.2. Cloudy-Sky Study

The cloudy comparisons are restricted to at most 15 different models for some cases, with no line-by-line benchmarks. Apparently, several of the clear-sky participants did not perform the cloudy calculations because of a misperception of the complexity

of the cloudy comparison (i.e., many models are not set up to use nonblack clouds, even if they are nonscattering). Many treated the 1-km-thick clouds as nonblack, but also nonscattering. However, the details of the various model calculations are not known as well as for the clear-sky study. Thus the ensemble of cloudy-sky longwave results must be viewed as marking the range of variation among models performing the same calculation. Nevertheless, we believe that the statistics on the comparisons cover the range of agreement between the various types of models used in many climate problems. The distributions of the model calculations of the downward flux at the surface ($F \downarrow$) and the upward flux at 13 km ($F \uparrow$) for the different cases are shown in Figures 19 and 20.

For the low cloud case (Figure 19), the spread of the flux calculations decreases as the clouds become nearly black (LWC of 200 g m^{-2}), with the great majority of the models agreeing to within 12 W m^{-2} . However, for optically thin clouds, the results for $F \downarrow$ are spread over a range of about 35 W m^{-2} . For $F \uparrow$, the spread increases over that found for clear-sky conditions, but most of the models are within a 12 W m^{-2} range. The outliers tend to differ in the same direction for each case. Overall, the relative intermodel differences are similar for clear and cloudy conditions for both $F \uparrow$ and $F \downarrow$.

With the cloud top at 13 km (Figure 20), the range of agreement of the $F \downarrow$ calculations is similar to that for $F \uparrow$ for the low cloud case, with all but one of the z-tested models falling within a 12 W m^{-2} range. However, with the exception of the near-black

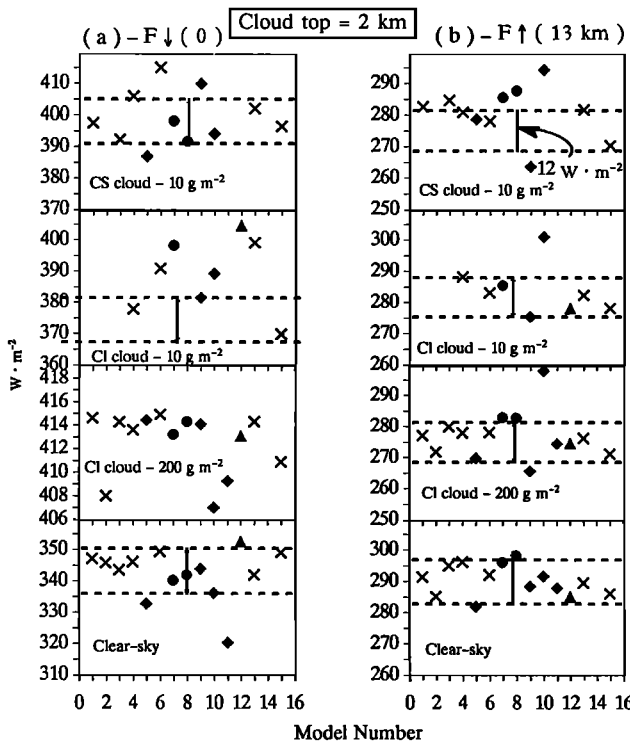


Fig. 19. Distributions of model calculations of (a) $F \downarrow$ at the surface and (b) $F \uparrow$ at 13 km for a 1-km-thick cloud topped at 2 km with the indicated cloud liquid water contents (or clear-sky conditions). The calculations use 300 ppmv CO_2 , and the H_2O , O_3 , and temperature distributions of the midlatitude summer atmosphere. Symbols are as in Figure 15.

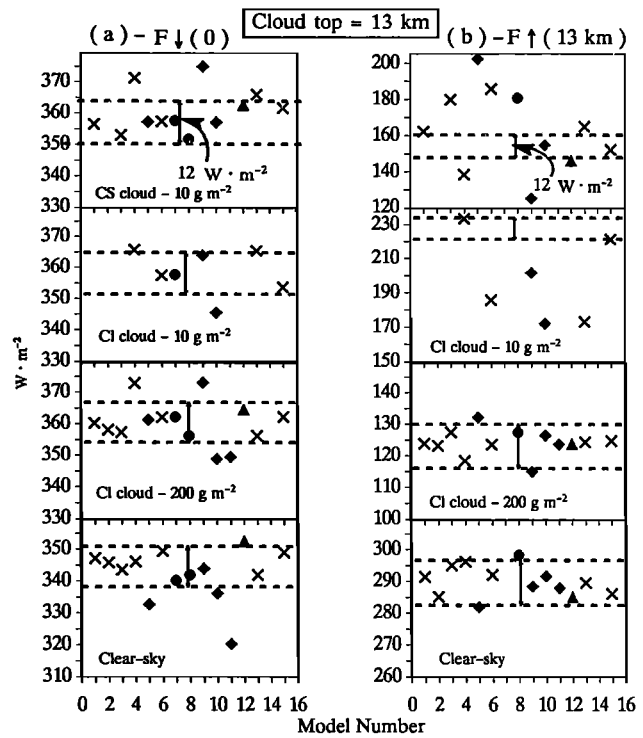


Fig. 20. As in Figure 19 but with the cloud top at 13 km.

cloud, the intermodel spread of $F \downarrow$ is larger for cloudy than for the clear-sky conditions.

For $F \uparrow$, the agreement between models becomes poor as the cloud becomes optically thin (Figure 20b). Since the model calculations of $F \uparrow$ tend to agree with each other relatively closely without clouds, the increased spread indicates that there are rather large disparities in the manner by which the clouds are treated. Note that model 15 treats the cloud scattering and absorption properties quite carefully. Thus the spread relative to that calculation is probably a good measure of the inadequacy of a given parameterization.

In general, for near-black clouds, the calculations agree more closely near the cloud boundaries than for the more transparent ones. Nevertheless, the range of fluxes of 35 W m^{-2} for $F \downarrow$ and 80 W m^{-2} for $F \uparrow$ for the relatively simple thin cloud cases is disturbingly large. The magnitudes of the ranges of the fluxes is comparable to the results for clear-sky cases.

The differences between the various model results for the cloudy cases have just begun to be studied. Some of the causes are undoubtedly related to those of the clear-sky study, with the added complexities of different treatments for calculating cloud radiative properties and multiple scattering. The untangling of the web of possible explanations will require a careful examination of the various assumptions and details of the numerical techniques used in each model.

4.3. Model Assessment

ICRCCM was intended in part to determine the range of differences between models, but not to determine "The Best" model. By being nonjudgmental, the participants cooperated in sharing their results with their colleagues. However, the ICRCCM participants have agreed to release their results for examination by the larger scientific community. This will inevitably

lead to ranking of the models relative to the LBL models. Such a ranking from the ICRCM results is difficult because of the designs of the various models, the large number of cases and the variety of variables studied. Nevertheless, we have attempted to categorize the model results relative to the LBL calculations according to those cases studied extensively, namely, $F \downarrow$, ΔF_{net} , and δF_{net} . The cloud cases are not considered because of the lack of an established benchmark and the small number of participants. Please note that this categorization is intended to be informational and not judgmental of the applicability of a given model to any specific purpose.

The categorization is based on the largest differences between model and LBL results for the five model atmospheres. By denoting $\delta F \downarrow$, $\delta \Delta F_{\text{net}}$ and $\delta \delta F_{\text{net}}$ as the absolute value of the differences between model and average line-by-line calculations of $F \downarrow$, ΔF_{net} , and δF_{net} , respectively, we have defined four categories as follows:

1. $\delta F \downarrow$ and $\delta \Delta F_{\text{net}} \leq 12 \text{ W m}^{-2}$ and
 $\delta \delta F_{\text{net}} \leq 0.6 \text{ W m}^{-2}$.
2. $\delta F \downarrow$ and $\delta \Delta F_{\text{net}} \leq 12 \text{ W m}^{-2}$ and
 $\delta \delta F_{\text{net}} > 0.6 \text{ W m}^{-2}$.
3. $\delta F \downarrow$ and/or $\delta \Delta F_{\text{net}} > 12 \text{ W m}^{-2}$ and
 $\delta \delta F_{\text{net}} \leq 0.6 \text{ W m}^{-2}$.
4. $\delta F \downarrow$ and $\delta \Delta F_{\text{net}} > 12 \text{ W m}^{-2}$ and
 $\delta \delta F_{\text{net}} > 0.6 \text{ W m}^{-2}$.

Relative to line-by-line calculations for mid-latitude summer conditions, 0.6 W m^{-2} is about 10% of δF_{net} , and 12 W m^{-2} is about 3.5% $F \downarrow$ and about 6% of ΔF_{net} . These categories are arbitrary, but for models based on spectral line data, we believe these limits represent a very liberal interpretation of the level of numerical, and absolute for CO₂, accuracy attainable with the available spectral data and numerical techniques. Table 13 lists the categorizations for wide and narrow band models, respectively. Note that in order to be listed, a model had to have completed the calculations for at least two of the three quantities.

Our interpretation of Table 13 is as follows. Those models in categories 1 and 2 appear to be reasonably performing the bulk calculations of tropospheric fluxes and heating rates. These modelers should devote their activities to ascertaining the reliability of vertical profiles of fluxes and heating rates through comparisons with LBL results. Modelers in categories 3 and 4 should devote additional action to improving their numerical techniques before advancing to tests of vertical profiles of fluxes and heating rates. Models in categories 1 and 3 are doing reasonably well for the sensitivity to CO₂, but models in categories 2 and 4 should reexamine their CO₂ parameterizations.

In summary, there are but a few wide-band models and several narrow-band models that yield results comparable to line-by-line models for clear-sky conditions to within rather liberal limits. However, no model can be arbitrarily trusted to give such agreement with line-by-line models unless great care is taken to accurately model the various integrals and unless the actual ICRCM comparisons are made.

5. CONCLUSIONS

The results of the update of the longwave clear-sky study and the results of the cloudy calculations reinforce many of the conclusions made previously [Luther et al., 1988], namely,

TABLE 13. Assessment of Model Results

Category	Investigator
<i>Narrow-Band Models</i>	
1	R. G. Ellingson, S. Gupta, J. Kiehl, J. Kiehl, W. Kuhn, J.-J. Morcrette, E. Smith, S. Tjemkes, and W. Wiscombe
2	A. Lacis
3	J.-P. Blanchet (RADSN) [*] , J. Schmetz [*] , and W.-C. Wang [*]
<i>Wide Band Models</i>	
1	S. Fels and D. Schwartzkopff [§] , S. Fels, (Sky-Hi) [†] , Harshvardhan [*] , R. E. Newell, and R. Wetherald [*]
2	J.-J. Morcrette, S. Fels (GFD-GCM 1988) [‡] , J. Kiehl and B. Briegleb (NCAR-CCM1), B. Ritter and J. Slingo (ECMWF - Full) [‡] .
3	K.-N. Liou and S. Ou [*] , K. Schine, A. Slingo-new [*] , and A. Slingo-old [*]
4	J.-P. Blanchet [*] , E. M. Feigelson [†] , S. Ghan (LLNSDCM) [†] , I. Karol [†] , F. Nieuwstadt and S. Tjemkes [*] , and M. E. Schlesinger [*]

^{*}Model not z-tested.

[Questionnaire not submitted for this model.

]Did not perform doubled CO₂ test.

wCalculations for only MLS atmosphere.

1. Different line-by-line model results tend to agree to within 1%. Nevertheless, those conducting such calculations do not believe that their results should be used as an absolute reference, due to uncertainties about line shape and absorption continua.

2. Medians of band model fluxes and cooling rates agree within 1-2% with LBL results. The revised and new model calculations added to the comparison, since the Frascati workshop have narrowed the overall agreement with the LBL results. However, there is a large variation among the models: 5 to 10% rms differences with LBL results.

3. Band model calculations of sensitivities to changes in absorbing constituents show poorer agreement with line-by-line results, and a much larger spread, than calculations of flux components.

4. In cases of CO₂ only and H₂O only, the spread among band models increases considerably, compared to the case when all absorbing gases are included; this indicates that our success in the latter case is partly fortuitous because of the way absorbing bands overlap in the Earth's atmosphere.

5. The H₂O continuum masks many differences between model results. Nevertheless, the continued absence of a widely accepted theory (and parameters) for it poses many limitations for studies of the climates of planetary atmospheres.

For the cloudy-sky calculations we must add to these conclusions as follows.

1. For near-black clouds, the calculations agree closely near the cloud boundaries. At levels removed from the boundaries, the differences resemble those from the clear-sky calculations.

2. There is a large spread among model calculations for optically thin clouds (the order of 35 to 80 W m⁻²) which are comparable to the results for clear-sky cases. However, the analysis indicates that these large disparities are related to the manner by which the clouds are treated in the models rather than to differences in the treatments of clear-sky absorption and emission.

The analysis of the results presented herein shows that the outliers to many of the clear-sky calculations appear to be related to those models that have not tested the techniques used to perform the integration over altitude. When these outliers are

removed, the agreement between narrow-band models and the line-by-line models is about $\pm 2\%$ for fluxes at the atmospheric boundaries, about $\pm 5\%$ for the flux divergence for the troposphere, and to about $\pm 5\%$ for the change of the net flux at the tropopause as CO₂ doubles. However, this good agreement does not extend to the majority of the models currently used in climate models. Only five wide-band models were found to match the performance of the narrow band models.

It should be noted that during the course of ICRCMM, changes have been and are continuing to be made to the radiation parameterizations at several of the internationally recognized centers of climate modeling activity. These include NCAR/CCM (H₂O, CO₂, O₃, and the continuum), UK Meteorological Office (H₂O and the continuum), GFDL(CO₂ and the continuum), ECMWF (ongoing changes of the entire code), NASA/GLA (H₂O, CO₂, and O₃), and LLNL (H₂O, CO₂, O₃, and the continuum).

The impact of these changes on the performances of the various climate models is difficult to ascertain because many other changes have also been made at the same time. Nevertheless, the ICRCMM activities have apparently played a major part in these modifications.

Although a great deal has been learned, the reasons for many of the model differences have not been explained. Most of the major variations between model results are believed to be due to using different widths of the spectral intervals, using different treatments of the H₂O continuum, errors in calculating the temperature dependence of spectral lines, errors in the numerical techniques used for integration over altitude, different sources of spectral line data, differences in the way band parameters are derived from spectral data, and differences in the manner for including cloud effects. The discovery of the exact causes for discrepancy between individual models will require a substantial study of each model.

To aid in the discovery of the causes of these differences, the ICRCMM participants have agreed to provide the results of their calculations and summary information about their models to the open scientific community. Preparations are under way to store these data in a convenient location for electronic access. In the interim, information on how to obtain the tabular listings and to participate in ICRCMM may be obtained from Ellingson.

As ICRCMM has progressed, there has been a substantial narrowing of the results as errors have been found in the various codes. These results indicate that we are in the marginal range of (relative) accuracy for calculating longwave flux quantities necessary for many climate programs, such as TOGA. However, it should be emphasized that not all such models will give such accuracy. The ICRCMM participants recommend that a code not be accepted to provide such accuracy until it has made comparisons to the line-by-line results of this study.

The 30–80 W m⁻² range of variation in longwave radiative flux computations discovered during this study are a significant fraction of normally observed latent and sensible energy fluxes. In the end it is these energy fluxes which control the climate. The reason that such large discrepancies in radiative fluxes have not seriously distorted model predictions of current climate is simply that most climate models are heavily tuned to give the "right answer" for current climate conditions. Although narrowing the differences between band and line-by-line models may be a useful exercise, without an absolute reference for comparison (i.e., a set of accurate and well documented, well-calibrated, spectral observations in the real atmosphere), radiation models may still lead to dangerous errors in the estimation of climatic impacts.

Therefore the ICRCMM participants recommend that a program be organized to simultaneously measure the spectral radiance at high spectral resolution along with the atmospheric variables necessary to calculate the radiance, particularly for clear-sky conditions. Only such detailed experiments can satisfactorily resolve the discrepancies that have been revealed by the ICRCMM study.

APPENDIX: TEST CASES AND ATMOSPHERIC DATA

The test cases for the clear and cloudy studies are described in Tables 3 and 4, respectively. The AFGL-based atmospheric data are listed in Tables 5 through 9. For each case, the upward, downward, and net flux components were compared at the Earth's surface, the tropopause, and the top of the atmosphere, and the tropopause for the different atmospheres was taken to be tropical, 17 km or 99.7 mbar; mid-latitude summer, 13 km or 179.0 mbar; mid-latitude winter, 10 km or 256.8 mbar; subarctic summer, 10 km or 267.7 mbar; subarctic winter, 9 km or 282.9 mbar.

The isothermal atmosphere calculations assumed the pressure distribution of the mid-latitude summer atmosphere. The calculations with the trace gases assumed mixing ratios for CH₄ and N₂O of 1.75 ppmv and 0.28 ppmv, respectively.

Acknowledgments. Each of the participants in ICRCMM has contributed a great deal of time to performing the computations summarized herein, and this work reflects a team effort by all of them. The analysis for this paper was funded in part by the U.S. Department of Energy's Carbon Dioxide Research Division through the Lawrence Livermore National Laboratory, and a portion of it was performed on the Apollo computer system located in the Department of Meteorology at the University of Maryland. Steven Fels contributed a section of this paper before his death.

REFERENCES

- Bignell, K. J., The water-vapour infra-red continuum, *Q. J. R. Meteorol. Soc.*, 96, 390–403, 1970.
- Burch, D. E., J. N. Howard, and D. Williams, Infrared transmission in synthetic atmospheres V: Absorption laws for overlapping bands, *J. Opt. Soc. Am.*, 46, 452–455, 1956.
- Burch, D. E., D. Grynkav, E. B. Singleton, W. L. France, and D. Williams, Infrared absorption by carbon dioxide, water vapor and minor atmospheric constituents, *Rep. 604-2633*, contract AF19, Ohio State Univ., Columbus, 1962.
- Chandrasekar, S., *Radiative Transfer*, 393 pp., Dover, New York, 1960.
- Chou, M.-D., and A. Arking, Computation of infrared cooling rates in the H₂O bands, *J. Atmos. Sci.*, 37, 855–867, 1980.
- Chou, M.-D. and L. Peng, A parameterization of the absorption in the 15 μm CO₂ spectral region with application to climate studies, *J. Atmos. Sci.*, 40, 2183–2192, 1983.
- Clough, S. A., F. X. Kneizys, and R. W. Davies, Line shape and the water vapor continuum in IRS '88: Current Problems in Atmospheric Radiation, edited by J. Lenoble and J.-F. Geleyn, pp. 355–359, A. DEEPAK, Hampton, Va., 1989.
- Curtis, A. R., The computation of radiative heating rates in the atmosphere, *Proc. R. Soc. London Ser. A*, 236, 156–159, 1956.
- Drayson, S. R., Atmospheric transmission in the CO₂ bands between 12 μ and 18 μ , *Appl. Opt.*, 5, 385–391, 1967.
- Ellingson, R. G., and J. C. Gille, An infrared radiative transfer model, part 1, Model description and comparison of observations with calculations, *J. Atmos. Sci.*, 35, 523–545, 1978.
- Elsasser, W. M., *Heat Transfer by Infrared Radiation in the Atmosphere*, Harvard Meteorol. Stud. 6, Harvard University Press, Cambridge, Mass., 1942.

- Fels, S. B., and D. Schwarzkopf, An efficient, accurate algorithm for calculating CO₂ 15-μm band cooling rates, *J. Geophys. Res.*, **86**, 1205–1232, 1981.
- Goody, R. M., A statistical model for water vapour absorption, *Q. J. R. Meteorol. Soc.*, **78**, 165–169, 1952.
- Goody, R. M., *Atmospheric Radiation I: Theoretical Basis*, 436 pp., Oxford at the Clarendon Press, London, 1964.
- Grassi, H., A new type of absorption in the atmospheric infrared window due to water vapor polymers, *Contrib. Atmos. Phys.*, **49**, 225–236, 1976.
- Haurwitz, F., and W. R. Kuhn, The distribution of tropospheric planetary radiation in the southern hemisphere, *J. Appl. Meteorol.*, **13**, 417–429, 1974.
- Hitchfeld, W., and J. T. Houghton, Radiative transfer in the lower stratosphere due to the 9.6 micron band of O₃, *Q. J. R. Meteorol. Soc.*, **87**, 562–577, 1961.
- Hoover, G. M., C. E. Hathaway, and D. Williams, Infrared absorption of overlapping bands of atmospheric gases, *Appl. Opt.*, **6**, 481–487, 1967.
- Hottel, H. C., and A. F. Sarofim, *Radiative Transfer*, McGraw-Hill, New York, 1967.
- Kiehl, J. T., and V. Ramanathan, Radiative heating due to increased CO₂: The role of H₂O continuum absorption in the 12–18 μm region, *J. Atmos. Sci.*, **39**, 2923–2926, 1982.
- Kiehl, J. T., and V. Ramanathan, CO₂ radiative parameterization used in climate models: Comparison with narrow band models and with laboratory data, *J. Geophys. Res.*, **88**, 5191–5202, 1983.
- Kneizys, F. X., E. P. Shettle, L. W. Abreu, J. H. Chetwynd, G. P. Anderson, W. O. Gallery, J. E. A. Selby, and A. A. Clough, Users Guide to Lowtran7, *Rep. AFGL-TR-88-0177*, 137 pp., Air Force Geophys. Lab., Hanscom, Mass., 1988.
- Lacis, A. A., and J. E. Hansen, A parameterization for the absorption of solar radiation in the Earth's atmosphere, *J. Atmos. Sci.*, **31**, 118–133, 1974.
- Lee, A. C. L., A study of continuum absorption in the 8–13 micron window, *Q. J. R. Meteorol. Soc.*, **99**, 490–505, 1972.
- Luther, F. M., R. G. Ellingson, Y. Fouquart, S. Fels, N. A. Scott, and W. J. Wiscombe, Intercomparison of radiation codes in climate models (ICRCM): Longwave clear-sky results—A workshop summary, *Bull. Am. Meteorol. Soc.*, **69**, 40–48, 1988.
- McClatchey, R. A., R. W. Fenn, J. E. A. Selby, F. E. Volz, and J. S. Garing, Optical properties of the atmosphere, *Rep. AFCRL-71-0279*, 85 pp., Air Force Cambridge Res. Lab., Bedford, Mass., 1971.
- McClatchey, R. A., W. S. Benedict, S. A. Clough, D. E. Burch, R. F. Calfee, K. Fox, L. S. Rothman, and J. S. Garing, AFCRL atmospheric absorption line parameters compilation, *Rep. AFCRL-TR-73-0096*, Air Force Cambridge Res. Lab., Bedford, Mass., 1973.
- Morcrette, J.-J., On the parameterization of radiation in general circulation models, Ph.D. dissertation 630, Univ. of Lille, France, 1984.
- Ramanathan, V., Radiative transfer within the Earth's troposphere and stratosphere: A simplified radiative convective model, *J. Atmos. Sci.*, **33**, 1330–1346, 1976.
- Roberts, R. E., L. M. Biberman, and J. E. A. Selby, Infrared continuum absorption by atmospheric water vapor in the 8–10 μm window, *Appl. Opt.*, **15**, 2085–2090, 1976.
- Rodgers, C. D., The radiative heat budget of the troposphere and lower stratosphere, *Rep. A2*, Mass. Inst. of Technol., Cambridge, 1967.
- Rodgers, C. D., and C. D. Walshaw, The computation of infrared cooling rates in planetary atmospheres, *Q. J. R. Meteorol. Soc.*, **92**, 67–92, 1966.
- Rothman, L. S., R. R. Gamache, A. Golman, L. R. Brown, R. A. Toth, H. M. Pickett, R. L. Poynter, J.-M. Flaud, C. Camy-Peyret, A. Barbe, N. Husson, C. P. Rinsland, and M. A. H. Smith, The HITRAN database: 1986 edition, *Appl. Opt.*, **26**, 4058–4097, 1987.
- Schack, A., The radiation from combustible gases and its practical determination, *Z. Tech. Phys.*, **5**, 267–278, 1924.
- Scott, N. A., and A. Chedin, A fast line-by-line method for atmospheric absorption computations: The automated atmospheric absorption atlas, *J. Appl. Meteorol.*, **20**, 801–812, 1981.
- Selby, J. E. A., E. P. Shettle, and R. A. McClatchey, Atmospheric transmittance from 0.25 to 28.5 μm: Supplement LOWTRAN 3B, *Rep. AFGL-TR-76-0258*, Air Force Geophys. Lab., Bedford, Mass., 1976.
- Stephens, G. L., Optical Properties of Eight Water Cloud Types *Tech. Rep. 36*, Commonwealth Sci. and Ind. Res. Org., Div. of Atmos. Phys., Aspendale, Australia, 1979.
- Tubbs, L. D., C. E. Hathaway, and D. Williams, Further studies of overlapping absorption bands, *Appl. Opt.*, **6**, 1422–1423, 1967.
- Wang, W.-C., and G.-Y. Shi, Total band absorptance and k-distribution function for atmospheric gases, *J. Quant. Spectrosc. Radiat. Transfer*, **39**, 387–397, 1988.
- World Meteorological Organization, The intercomparison of radiation codes in climate models (ICRCM), Longwave clear sky calculations, *Rep. WCP-93*, 37 pp., WMO World Climate Programme, Geneva, 1984.

R. G. Ellingson, Department of Meteorology, University of Maryland, 2213 Computer and Space Sciences Building, College Park, MD 20742.

J. Ellis, Lawrence Livermore National Laboratory, University of California, Livermore, CA 94550.

(Received September 5, 1989;
revised June 29, 1990;
accepted July 6, 1990.)